

UNCOVERING THE INTRINSIC VARIABILITY OF GAMMA-RAY BURSTS

V. ZACH GOLKHOU^{1,2} & NATHANIEL R. BUTLER^{1,2}

Accepted to ApJ

ABSTRACT

We develop a robust technique to determine the minimum variability timescale for Gamma-ray Burst light curves, utilizing Haar wavelets. Our approach averages over the data for a given GRB, providing an aggregate measure of signal variation while also retaining sensitivity to narrow pulses within complicated time-series. In contrast to previous studies using wavelets, which simply define the minimum timescale in reference to the measurement noise floor, our approach identifies the signature of temporally-smooth features in the wavelet scaleogram and then additionally identifies a break in the scaleogram on longer timescales as signature of a true, temporally-unsMOOTH light curve feature or features. We apply our technique to the large sample of *Swift* GRB Gamma-ray light curves and for the first time – due to the presence of a large number of GRBs with measured redshift – determine the distribution of minimum variability timescales in the source frame. We find a median minimum timescale for long-duration GRBs in the source frame of $\Delta t_{\min} = 0.5$ s, with the shortest timescale found being on the order of 10 ms. This short timescale suggests a compact central engine (3×10^3 km). We discuss further implications for the GRB fireball model and present a tantalizing correlation between minimum timescale and redshift, which may in part be due to cosmological time-dilation.

Subject headings: gamma-ray burst: general — methods: statistical, data analysis

1. INTRODUCTION

Gamma-Ray Burst (GRB) light curves show a remarkable morphological diversity. While a significant number of bright long bursts ($\sim 15\%$) exhibit a single smooth pulse structure, in most cases GRBs appear to be the result of a complex, seemingly random distribution of several pulses. Burst pulses are commonly described as having fast-rise exponential-decay (FRED) shapes (e.g., Fenimore et al. 1996). Parameterized analyses of pulse profiles have shown broad log-normal distributions among different bursts and even within a single burst (see, e.g., Norris et al. 1996; Bhat et al. 2012).

Several approaches have been utilized to characterize the distribution of power versus timescale for GRBs and other astrophysical sources. These include structure function (SF) analyses (Trevese et al. 1994; Hook et al. 1994; Cristiani et al. 1996; Aretxaga et al. 1997), autocorrelation function (ACF) analyses (Link et al. 1993; Fenimore et al. 1995; in't Zand & Fenimore 1996; Borgonovo 2004; Chatterjee et al. 2012), and Fourier power spectral density (PSD) analyses (Beloborodov et al. 2000; Chang 2001; Abdo et al. 2010; Guidorzi et al. 2012; Dichiara et al. 2013). In principle, the ACF contains the same information as the PSD, since one is the Fourier transform of the other (the Wiener-Khinchin theorem, Chatfield 2003). The SF is mathematically very similar to the ACF.

As Hawkins (2002) summarizes, the SF, ACF, and PSD – when calculated for a given dataset – are not completely equivalent because of time-windowing effects and the presence of measurement noise. For long runs of evenly spaced data, the PSD is used in preference to the ACF, as it can be easier to interpret and understand

errors. In cases of short or inhomogeneous data sets, the ACF can provide a more stable measurement. However, as ACF values at different time lags are not statistically independent of each other, the ACF interpretation may not be simple.

The first-order SF was introduced in astronomy by Simonetti et al. (1985). It has been widely used in the analysis of quasar light curves (e.g., Trevese et al. 1994; Hawkins 2002) and microlensing statistics (e.g., Wyithe & Turner 2001). Compared to power-spectral analyses, the SF approach is less dependent on the time sampling (Paltani 1999). Following these studies, we define the first-order SF as a measure of the mean square difference of a signal $X(t)$ on timescale (or “lag”) τ :

$$\text{SF}(\tau) = \langle [X(t) - X(t + \tau)]^2 \rangle \quad (1)$$

Here, $\langle \cdot \rangle$ denotes an averaging over t . In Figure 1, we reproduce the typical shape of an SF, from Hughes et al. (1992).

We will be primarily interested below in using the SF to infer the shortest timescale at which a GRB exhibits *uncorrelated temporal variability*. In a seminal study, Walker et al. (2000) (and more recently, MacLachlan et al. 2013) utilize Haar wavelet scaleograms to measure minimum timescales. Wavelets are a set of mathematical functions, which form an orthonormal basis to compactly describe narrow time features (e.g., Daubechies 1992; Norris et al. 1994; Kolaczyk 1997; Scargle et al. 2013). Making the connection between the Haar wavelet scaleogram and the SF, as we do below in mathematical detail, sheds new light on prior work, allowing for a more rigorous analysis and better physical interpretation of the signal power versus timescale. We also exploit the large sample of *Swift* GRBs with measured redshifts to perform this analysis, for the first time, in the GRB source frame.

A general feature we observe in our scaleograms, pro-

¹ School of Earth and Space Exploration, Arizona State University, Tempe, AZ 85287, USA

² Cosmology Initiative, Arizona State University, Tempe, AZ 85287, USA

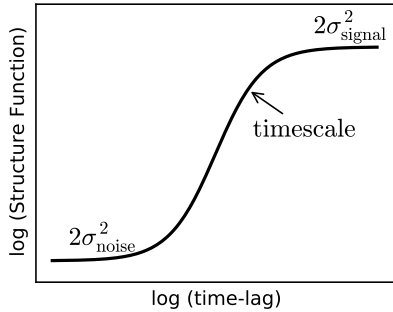


FIG. 1.— Schematic showing a typical SF for a time-series, from Hughes et al. (1992). At short lag-times, the SF flattens due to the measurements error. At long lag-times, the SF again flattens out at a level corresponding to the total variance in the signal. Between these lag-times, the slope of the SF depends on the noise properties of the signal and can be used to identify timescales of interest.

vided there is sufficient signal-to-noise ratio (SNR), is a linear rise phase relative to the Poisson noise floor on the shortest timescales (see, e.g., Figures 3 and 4). We take this to indicate a typical smoothness on the shortest observed timescales. We thus make an essential distinction – not made in prior studies – between correlated variability (i.e., smooth or continuous) and uncorrelated variability (e.g., pulses or changes in sign). For example, an exponentially decaying GRB light curve pulse with a fairly long time constant (say 100 s) will still exhibit power (i.e., yield a non-zero SF) on much shorter timescales (say 1 s), provided the SNR is sufficiently large for this to be measured. In contrast, the meaningful timescale (in this case ≈ 100 s and not 1 s) is the shortest timescale at which the signal becomes uncorrelated.

A simple Taylor expansion of the SF assuming a temporally-smooth signal $X(t)$, shown in Equation 2, elucidates how the minimum timescale for uncorrelated variability is connected to the scaleogram linear-rise phase.

$$X(t + \tau) = X(t) + \tau X'(t)|_{\tau} + \dots, \quad (2)$$

Substituting Equation 2 into Equation 1 and ignoring higher order terms produces Equation 3:

$$\sqrt{\text{SF}(\tau)} \propto \tau \quad (3)$$

which shows that for timescales where the signal is smoothly varying, we expect a linear dependence on the time lag τ . When the variation becomes non-smooth, SF flattens, providing a signature of the true GRB minimum timescale. Previous studies (Walker et al. 2000; MacLachlan et al. 2013) – which overlook the importance of the $\text{SF} \propto \tau$ region – incorrectly interpret the GRB minimum as the shortest timescale at which the SF is first non-zero (after subtracting the measurement noise level), potentially under-estimating the true variability timescales.

In this paper, we begin with a more detailed description of our method – the Haar wavelet structure function – which exploits a non-decimated, discrete Haar wavelet transform to estimate the SF and, in turn, the minimum variability timescale for a large number GRBs. We discuss the robustness of the structure function in extracting this timescale even in the case of complex GRBs con-

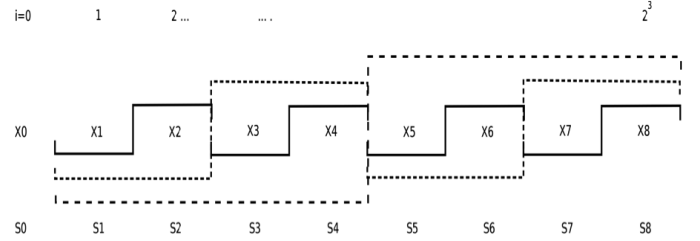


FIG. 2.— A schematic representation of relation between the Haar wavelet coefficients (Equation 6) and the first-order structure function. The Haar mother wavelet as shown step function (with different style) operates using scaling and dilation on a time-series: $\{X_i|i = 0.8\}$. $S_i = \sum_0^i X_i$.

taining multiple, overlapping pulses and we demonstrate self-consistency as the SNR is varied. Next, we apply the methodology to the full sample of GRBs observed by *Swift* BAT, summarizing the derived timescales for the population in the observer and GRB source frames. We conclude by discussing how these minimum variability timescales can elucidate the GRB central engine, help constrain models for the emission mechanism, and potentially also enable a measurement of cosmological time-dilation.

2. METHOD: A STRUCTURE FUNCTION ESTIMATED USING HAAR WAVELETS

The technique developed in this section was first used in Kocevski et al. (2007) to study the time-structure of X-ray flares following *Swift* GRBs. It is applicable to a broad range of time-series. Consider a time-series of length N that can be regarded as one portion of one realization from the stochastic process $\{X_t, t = 0, \pm 1, \dots, T\}$ (considering a unit sampling interval). Let

$$\bar{X}_t(\tau) = \frac{1}{\tau} \sum_{n=0}^{\tau-1} X_{t-n} \quad (4)$$

represent the sample average of τ consecutive observations, the latest one of which is X_t . The Allan (1966) variance at scale τ is denoted by $\sigma_X^2(\tau)$ and is defined to be half the mean square difference between adjacent non-overlapping $\bar{X}_t(\tau)$'s; i.e.,

$$\sigma_X^2(\tau) = \frac{1}{2} \langle [\bar{X}_t(\tau) - \bar{X}_{t-\tau}(\tau)]^2 \rangle \quad (5)$$

Note that the *Allan* variance at scale τ is a measure of the extent to which averages over length τ change from one time period of length τ to the next (Percival & Walden 2006). Comparing Equation 5 to Equation 1, we see that the *Allan* variance is related to the SF of the smoothed signal \bar{X}_t .

In order to see how Haar wavelets can be used to estimate the SF (see, Figure 2), we will now relate the Haar wavelet coefficients to the averages calculated in determining the *Allan* variance. Consider the discrete Haar wavelet transform (Percival & Walden 2006) of the time-series X_1, \dots, X_N , where we assume that the sample size N is a power of 2 so that $N = 2^q$ ($q > 0$). By definition, this transformation consists of $N - 1$ “detail” coefficients and one “smooth” coefficient $s_1 = \sum_{t=1}^N \frac{X_t}{N}$. The detail coefficients $d_{j,k}$ are defined for scales $k = 1, 2, 4, 8, \dots, N/2$

and - within the k th scale - for indices $j = 1, 2, 3, \dots, N/2k$ as

$$d_{j,k} \equiv \frac{1}{\sqrt{2k}} \left[\sum_{n=0}^{k-1} X_{2jk-n} - \sum_{n=0}^{k-1} X_{2jk-k-n} \right] \quad (6)$$

We can now state the relationship between the *Allan* variance and the Haar wavelet coefficients $d_{j,k}$. Using Equations 6, we have

$$d_{j,k} = (\frac{k}{2})^{(1/2)} [\bar{X}_{2jk}(k) - \bar{X}_{2jk-k}(k)] \quad (7)$$

Under the assumption that $E\{d_{j,k}\} = 0$ so that the variance of $d_{j,k}$ is equal to $E\{d_{j,k}^2\}$, an average of the wavelet coefficients squared on scale k provides a natural estimator for the *Allan* variance:

$$\text{var}\{d_{j,k}\} = \langle d_{j,k}^2 \rangle = \frac{k}{2} \left\langle [\bar{X}_{2jk}(k) - \bar{X}_{2jk-k}(k)]^2 \right\rangle = \tau \sigma_X^2(\tau) \quad (8)$$

We will redefine our wavelet coefficients (Equation 6) by dividing out another factor of $\sqrt{k/2}$, eliminating the k dependence in Equation 8.

2.1. Data Analysis and Haar-SF Implementation

In this section, we further develop our algorithm and discuss its application to GRB data captured by NASA's *Swift* satellite (Gehrels et al. 2004). Our automated pipeline at Arizona State University is used to download the *Swift* data in near real time from the *Swift* Archive³ and quicklook site. We use the calibration files from the 2008-12-17 BAT database release. We establish the energy scale and mask weighting for the BAT event mode data by running the `bateconvert` and `batmaskwtevt` tasks from the HEASoft 6.12 software release⁴. The mask weighting yields background-subtracted light curves. Light curves are extracted in the 15–350 keV band using the `batbinevt` tool with 100 μs time bins, applying a uniform random deviate on the same timescale to undo artifacts associated with the data capture⁵. The burst duration intervals are determined automatically as described in Butler et al. (2007).

Next, we group together adjacent time bins in the light curve until each composite bin has a fixed SNR of 5, dividing by the exposure time contained with each composite bin to produce the count rate versus time. We then apply our analysis to the natural log of the binned light curve so that the error per light curve bin is approximately constant. For homoscedastic errors – as we now have – the orthogonality properties of the Haar wavelets lead to approximate statistical independence of the wavelet coefficients (see, e.g., Percival & Walden 2006). We find that working with binned data with approximately constant errors from point to point leads to the most stable SF estimates.

Producing a scaleogram using the logarithm of the count rate can be interpreted as yielding the average *fractional* change in the signal versus timescale. We believe such a measure allows for more physical insight into the

emission mechanism than a measure of absolute change versus timescale. We note that the time binning will no longer be uniform. This is not a problem for the analysis, provided we propagate the true time difference associated with each wavelength coefficient through the analysis. We call the resulting scaleogram the Haar wavelet structure function, and we will denote it as $\sigma_{X,\Delta t}$ below. To improve statistics, we calculate $\sigma_{X,\Delta t}$ using not just one discrete Haar transform, but averaging $\sigma_{X,\Delta t}$ over the N transforms resulting from cyclic permutations of the data of length N (i.e., the non-decimated Haar transformation).

2.2. A Sample Burst: The “Naked-Eye” GRB 080319B

We now implement the Haar structure function on a real GRB light curve. The prompt BAT Gamma-ray light curve for GRB 080319B (see, e.g., Bloom et al. 2009, and references therein) and our derived $\sigma_{X,\Delta t}$ curve are shown in Figure 3. To guide the eye, several lines of constant $\sigma_{X,\Delta t} \propto \Delta t$ are also plotted. The expected measurement error has been subtracted away, leaving only the fractional flux variation expected for the GRB. On timescales where this net variation is greater than zero at the 3σ confidence level, we plot data points. Otherwise we plot upper limits.

Although there is excess signal present on timescales as short as 20 ms in Figure 3 (bottom), these timescales correspond to a region of the plot where $\sigma_{X,\Delta t} \propto \Delta t$ and should be interpreted as being due to temporally-smooth variations in a signal which is varying in an unsmooth fashion on longer timescales. The $\sigma_{X,\Delta t}$ points pull away significantly (2σ level from a $\Delta\chi^2$ test) from the $\sigma_{X,\Delta t} \propto \Delta t$ curve at $\Delta t_{\min} = 40 \pm 10$ ms. This is the timescale of interest, describing the minimum variability time for uncorrelated variations in the GRB.

Beyond this timescale, $\sigma_{X,\Delta t}$ is flatter than $\sigma_{X,\Delta t} \propto \Delta t$, indicating the presence of pulses with typical durations on these timescales. On a timescale of about 1 s, the $\sigma_{X,\Delta t}$ begins turning over due to a lack of signal variation between this timescale and the timescale (tens of seconds) describing the emission envelope. We are not concerned here with those longer timescale structures, although we do note that $\sigma_{X,\Delta t}$ provides a rich, aggregate description of this temporal activity.

In the inset to Figure 3 (top), we show a zoom-in on the narrowest time structure present in the signal. It can be seen that the approximate rise-time of this pulse corresponds nicely to our derived minimum timescale.

2.3. Simulated GRBs

The above example demonstrates that $\sigma_{X,\Delta t}$ can be used to extract a minimum timescale from a bright GRB with a rich temporal profile. How robust would the recovery of this timescale be for fainter GRBs? We examine this question using simulated pulses. Figure 4 displays a simulated GRB, consisting of a single pulse with FRED profile. The minimum timescale – corresponding to the rise of the pulse – can be correctly identified because there is sufficient SNR to identify the $\sigma_{X,\Delta t} \propto \Delta t$ region of the plot preceding that timescale.

We now consider a pulse with markedly different rise-time T_{rise} and total duration T_{tot} , over a range of possible brightness. Figure 5 shows a simulated GRB (single

³ <ftp://legacy.gsfc.nasa.gov/swift/data>

⁴ <http://swift.gsfc.nasa.gov/docs/software/lheasoft/download.html>

⁵ See, http://swift.gsfc.nasa.gov/docs/swift/analysis/bat_digest.html

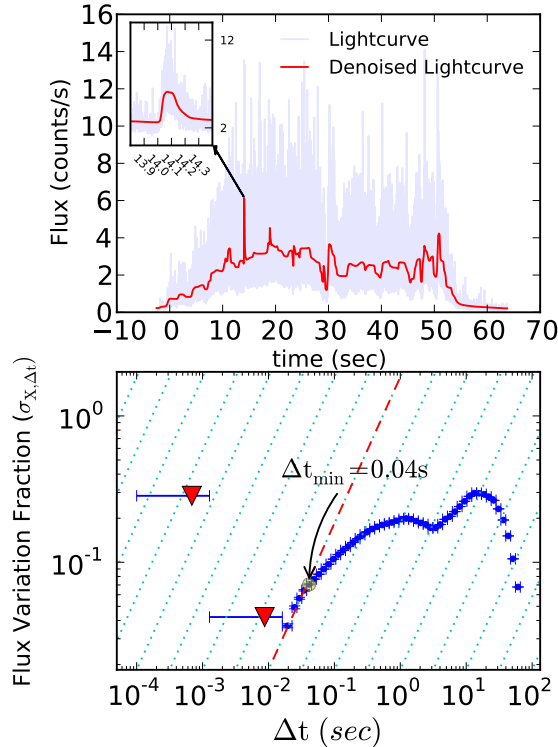


FIG. 3.— (Top) *Swift* BAT light curve (15–350 keV band) of the “Naked Eye” GRB 080319B. Overplotted is a denoised version of the light curve (following Kolaczyk (1997), see also Quilligan et al. (2002)), highlighting the true signal variation that would be observed were there no Poisson error on the measurement. (Bottom) The Haar wavelet scaleogram $\sigma_{X,\Delta t}$ vs. timescale Δt for GRB 080319B. We show only 3σ excesses over the power associated with Poisson fluctuations and report lower values as 3σ upper limits using red triangles. We derive a minimum timescale of 40 ± 10 ms (Section 2.2), corresponding to the shortest timescale at which $\sigma_{X,\Delta t}$ departs from $\sigma_{X,\Delta t} \propto \Delta t$. The corresponding light curve structure can be seen clearly in the top panel inset.

pulse) with $T_{\text{rise}}/T_{\text{tot}} \sim 1/100$. The left panel shows a pulse which is an order of magnitude brighter than that in the right panel. The bottom panels of Figure 5 display the corresponding fractional flux variation $\sigma_{X,\Delta t}$ as a function of timescale Δt . The derived minimum timescale in case of brighter light curve is close to the rise-time of 1 s.

When we decrease the pulse SNR, the linear rise phase spans less of the plot and is harder to identify (Figure 5 (right)); it becomes more difficult to identify the minimum timescale. In this example, Δt_{\min} is still identified correctly for 10 times lower SNR. We note that the y-axis levels ($\sigma_{X,\Delta t}$) in the low and high SNR plots are consistent: we infer the correct fractional signal power at each Δt in each case.

With further decreasing SNR levels, the linear rise phase in $\sigma_{X,\Delta t}$ due to the pulse rise will become absent. If the first non-zero $\sigma_{X,\Delta t}$ values lies on a line flatter than linear, the associated Δt_{\min} value must be regarded as an upper limit. We will follow this convention below: if a linear rise phase on the shortest timescales cannot be confirmed, Δt_{\min} will be taken as an upper limit.

At very low SNR levels, our analysis will tend to miss

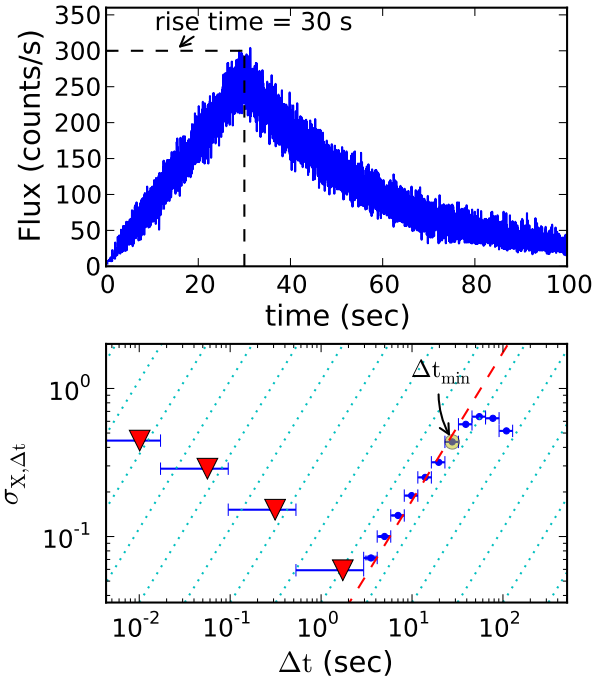


FIG. 4.— A simulated FRED pulse with a rise time of 30 s (Top) and the corresponding Haar wavelet scaleogram $\sigma_{X,\Delta t}$ vs. timescale Δt (Bottom). The expected Poisson noise level has been subtracted. The scaleogram rises linearly on short timescales corresponding to regions of the light curve where the signal is varying smoothly, falling away from the $\sigma_{X,\Delta t} \propto \Delta t$ trend on a timescale (≈ 30 s). This minimum timescale can be robustly measured, provided there is sufficient SNR for the linear region preceding it to be well identified.

the linear rise phase in $\sigma_{X,\Delta t}$ associated with the pulse rise time and will instead identify the pulse decay time (or total GRB duration) as the minimum timescale. Because actual GRB pulses tend to be asymmetric like this simulated pulse, we expect our $\sigma_{X,\Delta t}$ analysis to correctly identify true minimum timescale if it is within an order of magnitude (or so) of the lowest measurable timescale. Care will have to be taken when considering faint GRBs with $\sigma_{X,\Delta t}$ of order unity and with Δt_{\min} comparable to the event duration.

We conclude from this that the measurement of a linear rise phase in $\sigma_{X,\Delta t}$, followed by a flattening, will allow us to infer the presence of a characteristic timescale describing the transition from smooth (correlated) to unsmooth (uncorrelated) variability. However, we will not generally be able to rule on the presence of uncorrelated variability on much shorter (i.e. factor 10–100) timescales. We stress again that the shortest timescale exhibiting a net $\sigma_{X,\Delta t}$ over the Poisson level (called Δt_{snr} below), is not a timescale with intrinsic meaning independent of the noise level.

3. DISCUSSION AND RESULTS

We analyze the *Swift* data set up until October 27, 2013, which consists of 744 GRBs, 251 with measured redshifts. We only consider those GRBs with total light curve SNR ≥ 10 , leaving 517 GRBs. Of these, we are able to confirm the presence of a linear rise phase in $\sigma_{X,\Delta t}$ on short timescales for 281 GRBs. We quote upper-limit

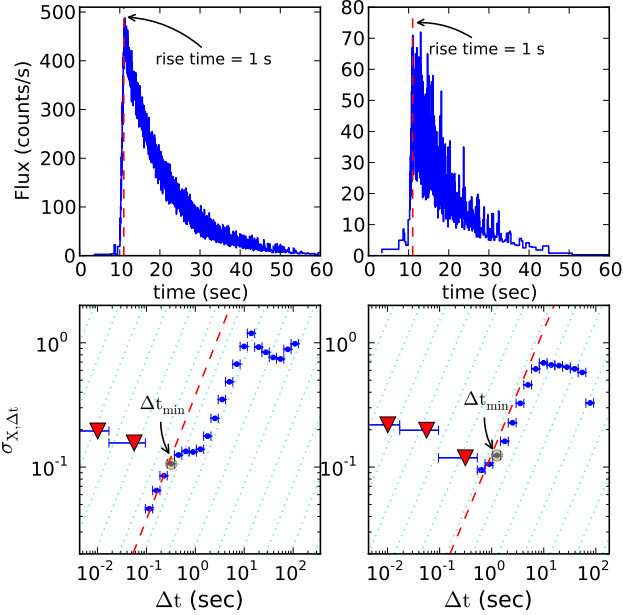


FIG. 5.— Simulated FRED pulses with a rise time of 1 s (Top). The left pulse is an order of magnitude brighter than the right pulse. The bottom panels show the corresponding Haar wavelet scaleogram $\sigma_{X,\Delta t}$ vs. timescale Δt . The expected level for Poisson noise has been subtracted. It is clear that fine-time structure can be missed in the low SNR limit; however the $\sigma_{X,\Delta t}$ measurements remain consistent.

values for the remainder. Most (256) of the bursts in this compiled subsample are long-duration ($T_{90} > 3$ s) GRBs. In the compiled subsample, 98 GRBs in the compiled subsample have measured redshift. The temporal specifications of all 517 GRBs discussed here are determined using fully-automatic software and are presented in Table 1. Light curves and Haar scaleograms are shown for a subset of the GRBs in Figure 6.

Figure 7 displays our minimum variability timescale, Δt_{\min} , versus the GRB duration, T_{90} . The short and long-duration GRBs are shown with diamond and circle symbols, respectively. In this plot the relative size of symbols is set by the ratio between minimum variability and SNR timescale ($\Delta t_{\min}/\Delta t_{\text{snr}}$). As described above, Δt_{snr} represents the first statistically significant timescale in the Haar wavelet scaleogram. The color of the points in Figure 7 corresponds to the fractional flux variation level ($\sigma_{X,\Delta t}$) at Δt_{\min} . A curved black line is also plotted to show a typical value for the minimum observable time (Δt_{snr}) versus the GRB duration, T_{90} (from Butler et al. 2007, 2010; Butler 2013).

We first note from the colors in Figure 7, that GRBs with Δt_{\min} close to T_{90} tend to have flux variation fractions of order unity. These are bursts with simple, single-pulse time profiles. As can be seen from the range of point sizes in Figure 7, most are not simply low SNR events where fine time structure cannot be observed. Also, we see that there are GRBs with both high and low SNR which have complex time-series ($\Delta t_{\min} \ll T_{90}$). Based again on the point colors, this short-timescale variation tends occur at a small fractional level in the signal ($\sigma_{X,\Delta t} \approx 1\text{--}10\%$), at least for the long-duration GRBs.

From a Kendall's τ -test (Kendall 1938), we find only

marginal evidence that Δt_{\min} and T_{90} are correlated ($\tau_k = 0.38$, 1.5σ above zero). The correlation strength is marginally stronger if we utilize the robust duration estimate T_{R45} (Reichart et al. 2001) in place of T_{90} : $\tau_k = 0.6$ (2.4σ). The Δt_{\min} values in Figure 7 are bound from above by T_{90} , and they do not strongly correlate with T_{90} within the allowed region of the plot. Recently, MacLachlan et al. (2013) have studied faint Fermi GBM GRBs and do find evidence for a correlation. We can reconcile our conclusions by identifying low SNR as the driving force in any apparent correlation. If we perform a truncated Kendall's τ test which only compares GRBs above one-another's threshold (Lloyd-Ronning & Petrosian 2002), the correlation strength drops precipitously ($\tau_k = 0.14$, 0.5σ for T_{90} ; $\tau_k = 0.4$, 1.5σ for T_{R45}). We, therefore, believe there is no strong evidence supporting a real correlation between Δt_{\min} and T_{90} .

Figure 8 (left) shows histograms for the *Swift* GRBs with reliable Δt_{\min} (in blue) measurement and also the GRBs for which only upper limits on Δt_{\min} could be derived (in red). The distributions have consistent mean values. (We discuss discrepancies between the tails of the distributions below.) We find a median minimum timescale for long-duration (short-duration) GRBs in the observer frame of 2.5 s (0.2 s). In the source frame, we find a median minimum timescale for long-duration (short-duration) GRBs of 0.5 s (2.1 s).

From Figure 8, we observe that the Δt_{\min} distribution of long-duration GRBs is displaced from that of short-duration GRBs (8σ , t -test). This finding is consistent with the findings of MacLachlan et al. (2013, see also Norris et al. (2001)), but not those of Walker et al. (2000) who find statistically indistinguishable distribution centers. We do note that the distribution centers appear to be consistent when viewed in the source frame (Figure 8 (right)), although the number of short-duration GRBs with redshift is low. The reason for the observer frame discrepancy is likely the fact that short-duration GRBs tend to be detected only at low-redshift, unlike long-durations GRBs which span a broad range of redshifts.

Examining the dispersion in $\log(\Delta t_{\min})$ values, shows no strong evidence for dissimilar values for the long and short-duration samples ($< 1.5\sigma$, F -test). This finding is fully consistent with MacLachlan et al. (2013), where it was also found (using a larger sample of short-duration GRBs) that the two histograms are quite broad and very similar in dispersion.

We have a large sample of GRBs for which no Δt_{\min} could be calculated or for which only upper limits on Δt_{\min} were obtainable. To account for the relative frequencies of such GRBs, we employ a survival analysis (see, e.g., Feigelson & Nelson 1985). Figure 9 displays the Kaplan-Meier estimator curves, which combine the detections and upper limits. There are three thin curves (green, red, and gray) in each panel of Figure 9. The green curve is calculated including the derived upper limits for Δt_{\min} when SF fitting was possible. The red curve includes these as well as Δt_{\min} estimates for the remaining GRBs, where we take T_{90} as the limiting value of Δt_{\min} when no SF fitting was possible. The gray curve is similar to the red curve, with T_{R45} used in place of T_{90} for the limiting value of Δt_{\min} . The median minimum timescale for GRBs (long and short-duration) in the ob-

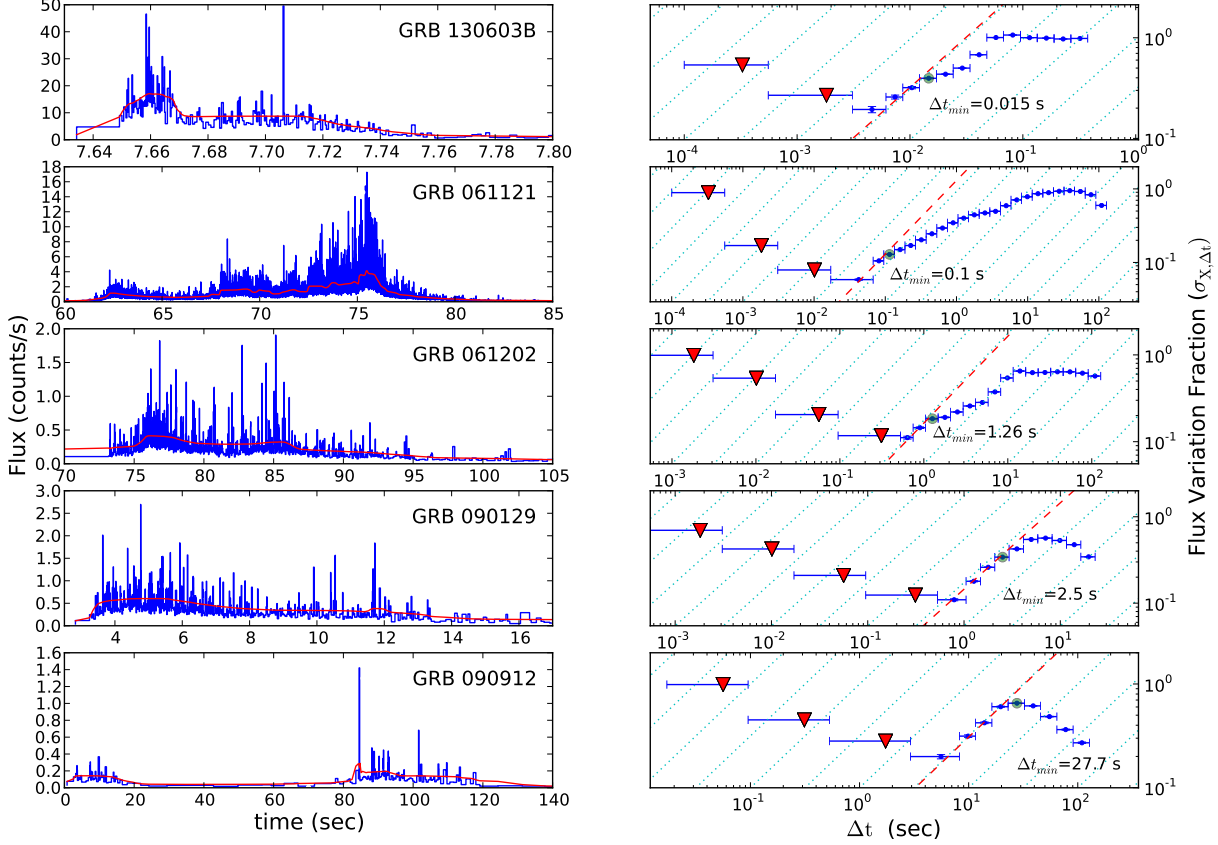


FIG. 6.— A gallery of Haar scaleograms $\sigma_{X,\Delta t}$, spanning a range of minimum variability timescale Δt_{\min} . The left panel shows the light curve in blue, with a denoised red curve to guide the eye (following Kolaczyk 1997). The corresponding Haar scaleogram plot is shown in the right panel. In each of these, the red dashed-line represents the temporally-smooth ($\sigma_{X,\Delta t} \propto \Delta t$) region and the green circle marks the extracted Δt_{\min} .

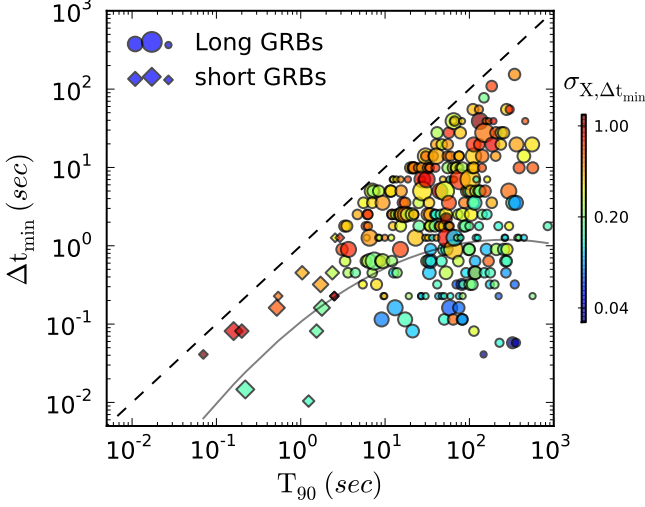


FIG. 7.— Our GRB minimum time Δt_{\min} plotted versus the GRB T_{90} duration. Circles (diamonds) represent long-duration (short-duration) GRBs. The point colors represent the fractional flux variation level ($\sigma_{X,\Delta t_{\min}}$) at Δt_{\min} . Also plotted as a curved line is the typical minimum observable Δt_{\min} as a function of T_{90} . The symbol sizes are set by the ratio of Δt_{\min} to the actual minimum observable time (Δt_{snr}) for each GRB.

server frame is $\Delta t_{\min} = 1.8$ s. In the source frame, the median is $\Delta t_{\min} = 0.5$ s. The survival analysis does not strongly affect these median values.

Walker et al. (2000), using BATSE data, report that most GRBs appear to exhibit millisecond variability. Claims have also been made for the presence of sub-millisecond variability (Bhat et al. 1992), and even microsecond variability (Mitrofanov (1989), but see Schaefer et al. (1993); Deng & Schaefer (1997)). In contrast, we find that only 0.4% of *Swift* BAT GRBs with well-measured Δt_{\min} have $\Delta t_{\min} < 10$ ms (observer frame). If we include all *Swift* GRBs using the survival analysis, we still find a fraction below 6% using T_{90} and below 15% using T_{45} . In the source frame, the numbers are 1% (well-measured) and 4% (all, using T_{90}) and 5% (all, using T_{45}). Of 517 bursts where 1 ms variability could have been measured, none show such short-timescale variability. We conclude that millisecond variability may be quite rare.

3.1. Evidence for Time-Dilation?

Given that we can derive a robust GRB minimum timescale and that redshifts have been measured for many of our GRBs, it is interesting to test whether these quantities are correlated. As GRBs are present over a very broad redshift range the signature of time-dilation ought to be present in GRB time-series. However, finding such a signal has remained elusive (Norris et al. (1994);

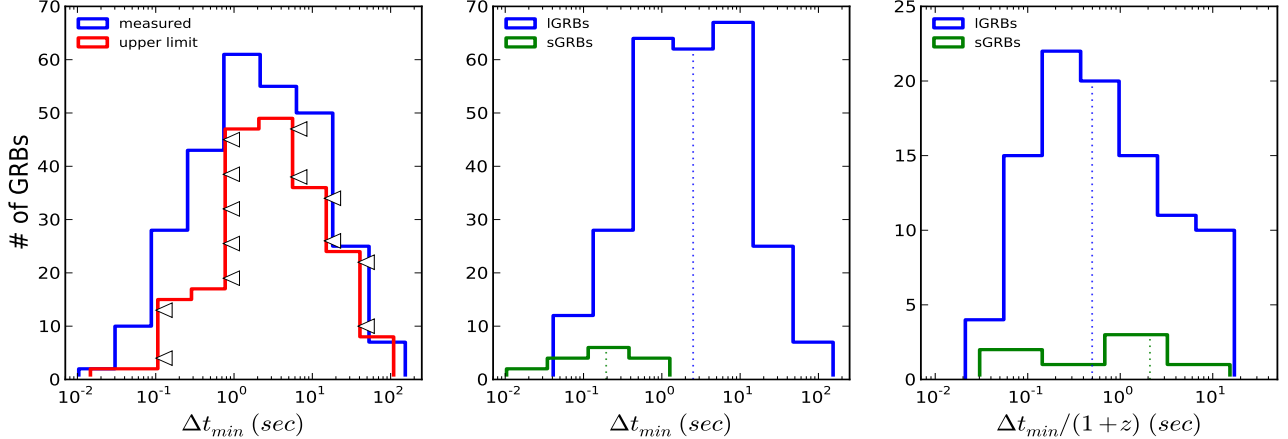


FIG. 8.— The histograms of Δt_{\min} with reliable measurement (blue) and for GRBs allowing for upper limits only (red). In observer frame (middle panel) the median minimum timescale for long-duration GRBs is: $\Delta t_{\min} = 2.5$ s, and for short-duration GRBs is $\Delta t_{\min} = 0.2$ s. The same quantities in source frame (right panel) are: $\Delta t_{\min} = 0.5$ s and $\Delta t_{\min} = 2.1$ s.

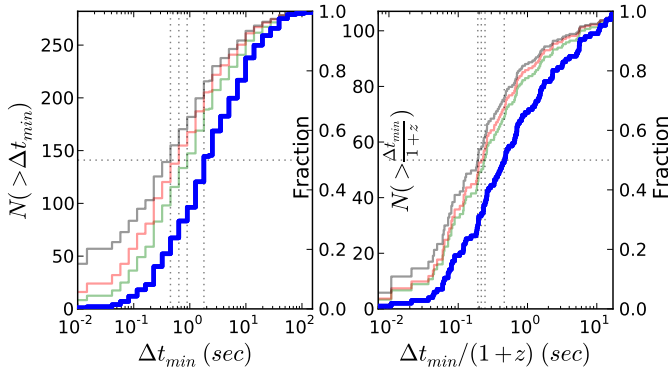


FIG. 9.— Cumulative distributions in the observer frame (left) and source frame (right) for Δt_{\min} for GRBs with well measured values (blue). The Kaplan-Meier estimator (Feigelson & Nelson 1985) is used to also include GRBs with upper limits on Δt_{\min} (green, red, and gray curves). The median minimum timescale for GRBs with long and short-durations in the observer frame is: $\Delta t_{\min} = 1.8$ s, and in source frame is: $\Delta t_{\min} = 0.5$ s.

Kocevski & Petrosian (2013), but see, e.g., Zhang et al. (2013)).

In Figure 10, we plot Δt_{\min} as a function of redshift. Redshift values are taken from Butler et al. (2007, 2010, and references therein). The blue crosses in Figure 10 correspond to geometric averages for sets of 10 bursts of similar redshift. The unbinned data are plotted in the background. We find that the binned data can be well-fitted by a line $\Delta t_{\min} = 0.3(1+z)^{1.6 \pm 0.4}$, possibly indicating the presence of time-dilation, although with a larger best-fit power-law index than would naively be expected. The effects of widening pulse width with decreasing observed energy bandpass (as a result of increasing redshift) are expected to play a role in increasing our observed index relative to that predicted from cosmological time dilation only (see, Fenimore et al. 1995; Norris et al. 1996).

The purity of this relation comes into question, however, when we perform a similar fit to the minimum observable timescale. We find that this quantity also correlates with redshift, as $\Delta t_{\text{snr}} = 0.2(1+z)^{1.2 \pm 0.3}$.

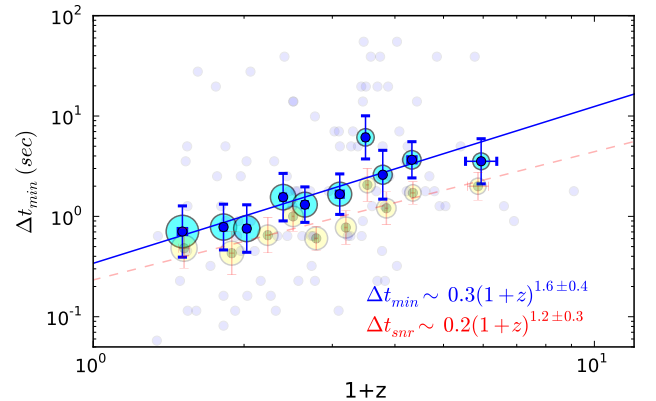


FIG. 10.— Minimum variability timescale in the observer frame versus redshift z . The blue crosses show geometric averages of Δt_{\min} with 10 bursts in each bin and red crosses show geometric averages of Δt_{snr} with 18 bursts in each bin. Cyan and yellow circles correspond to the average of SNR of bursts in each bin. The faint blue circles show all GRBs with measured Δt_{\min} and known z .

This must be the result of selection effects: more distant GRBs are fainter, thus permitting measurement of only long variability timescales. The power-law indices of the two fits are statistically consistent ($1-\sigma$ level). For the unbinned data, we find $\tau_k = 0.24$ (3.6σ), but this drops to $\tau_k = -0.02$ accounting for the limits. Given the clear role the threshold plays in defining the correlation strength, we cannot be confident that time-dilation is being uniquely measured by Δt_{\min} .

4. CONCLUSIONS

Using a technique based on Haar wavelets, we have studied the temporal properties of a sample of GRB hard X-ray, prompt-emission light curves captured by the BAT instrument on *Swift* prior to October 27, 2013. Our approach averages over the time-series captured for a given GRB, providing robust measures of minimum variability timescales.

In contrast to previous studies (Walker et al. 2000; MacLachlan et al. 2013; Bhat 2013), which simply de-

fine the minimum timescale in reference to the measurement noise floor, our approach identifies the signature of temporally-smooth features in the wavelet scaleogram and then additionally identifies a break in the scaleogram on longer timescales as signature of a true, temporally-unsmooth light curve feature or features. We find that this timescale (Δt_{\min}) tends to correspond to the rise-time of the narrowest GRB pulse (see, also, Bhat 2013).

We find a median minimum timescale for long-duration GRBs in the source (observer) frame of $\Delta t_{\min} = 0.5$ s ($\Delta t_{\min} = 2.5$ s). A consistent value in the source-frame for short-duration GRBs may indicate a common central engine.

We find that very few – at most 15% (5%) in the observer frame (source frame) – of *Swift* GRBs can have minimum timescales below 10 ms. Our timescales are thus considerably longer than the millisecond variability timescales found by Walker et al. (2000) to be common in bright BATSE GRBs. Partial explanation for this discrepancy must come from the fact that *Swift* BAT operates in a lower photon energy range than BATSE, and GRB pulses are known to be more narrow in higher energy bandpasses (e.g., Norris et al. 1996; Fenimore et al. 1995, 1996). Nonetheless, we note that the variability found in Walker et al. (2000) is not linked to the presence of discernible features in a given light curve (e.g., the pulse rise-time, which it is actually stated to be considerably less than). Given our new distinction between a Walker et al. (2000) type timescale (which we call Δt_{snr}) – the minimum possible observable Δt_{\min} for a GRB of given brightness and not necessarily the true Δt_{\min} – it is natural to expect that Walker et al. (2000) have underestimated their minimum timescales. We note that our minimum timescales are broadly consistent with those found in pulse-fitting studies (e.g., Fenimore et al. 1995; Norris et al. 1996).

4.1. Constraints on the Fireball Model

The standard fireball model postulates the release of a large amount of energy by a central engine into a concentrated volume (Cavallo & Rees 1978; Piran 2004), which causes the resulting outflow to expand and quickly become relativistic (Paczynski 1986). These relativistic expanding shells – with different Lorentz factors – in general collide, resulting in Gamma-ray flares and potentially rich temporal structure. Our extracted timescales (Δt_{\min}) should provide a diagnostic on the central engine power and its evolution. The size of the central engine is limited to $R < c \Delta t_{\min}$, which for the smallest minimum variability timescale derived above (~ 10 ms; see also, Nakar & Piran 2002) is $R < 3 \times 10^3$ km. Typical Δt_{\min} values from above lead to $R < 2 \times 10^5$ km. For the first time, due to a large sample of GRBs with measured redshift, we are able to perform these calculations in the source frame.

In the source frame, we are not able to confirm that the minimum variability timescale of short-duration GRBs is substantially shorter than that of long-duration. Hence, we cannot demonstrate that short-duration GRBs have a more condensed central engine than the former (see, Bhat 2013).

We can derive additional constraints on the GRB emission region, following the discussion in Walker et al.

(2000).

In the “external shock” picture, shells of material produced by the GRB impact material in the external medium. The physical dimension of clouds and their patchiness – in the direction perpendicular to the expansion of the shell – is constrained by Δt_{\min} . If we assume a single shell expanding at very close to light speed, the arrival time for photons from the shell will be calculated as the summation of travel time of the shell to the radius of impact and the travel time of the Gamma-rays to Earth. Photons from off-axis regions of the relativistic expanding shell experience a purely geometrical delay compared with photons from on-axis regions (Piran 2004) reaching the observer. The observed delay depends only on the radius of the shell R at the time of impact with a cloud in the external medium and the angular radius of the Gamma-ray emission region as subtended from the burst site ($\Delta\Theta$).

Walker et al. (2000) report millisecond variability superposed on pulses of significantly longer rise-times. High cloud patchiness can potentially explain this modulation, implying $\Delta\Theta < \Delta t_{\min}/(2\Gamma T_{\text{rise}}) < 0.0002$ radians, where Γ is the bulk Lorentz factor. Only $\sim 5 \times 10^{-3}$ of the emitting shell is active at a given time (also, Fenimore et al. 1999). However, for the bursts in our sample, with typical minimum variability timescale ~ 0.1 s, $T_{\text{rise}} > 1$ s, and assuming $\Gamma > 100$, we find that $\Delta\Theta < 5 \times 10^{-3}$ radians which is comparable with the typical surface filling factor (Fenimore et al. 1999).

In terms of the external shock scenario, the extracted Δt_{\min} can circumscribe the size scale of the impacted cloud along the line of sight. For a thin shell, the Gamma-ray radiation will start when the relativistic shell hits the inner boundary of the cloud with the peak flux produced as the shell reaches the densest region or center of the cloud. The size scale of the impacted cloud is limited by $2\Gamma^2 c \Delta t_{\min}$ since the shock is moving near light speed (Fenimore et al. 1996). For the smallest Δt_{\min} found ~ 10 ms, and assuming $\Gamma < 1000$, the cloud size must be smaller than 40 AU.

In the “internal shock” scenario (e.g., Rees & Meszaros 1994), the relativistic expanding outflow released from a central engine is assumed to be variable, consisting of multiple shells of differing Γ . These shells propagate and expand adiabatically until a faster shell collides with a slower one, resulting in a measurable rise time. This rise time to an outside observer would appear as: $\Delta t_{r1} \approx \Delta R / 2c\Gamma_1^2$, where ΔR and Γ_1 are the thickness and resulting Lorentz factor of the merged shell (e.g., Kocevski et al. 2007). Assuming the same scenario but for two other shells yields $\Delta t_{r2} \approx \Delta R / 2c\Gamma_2^2$. Writing $\Delta\Gamma = \Gamma_1 - \Gamma_2$, we have $\Delta\Gamma/\Gamma \approx 1/2(\Delta t_{\min}/T_{\text{rise}})$. In Walker et al. (2000), the ratios $\Delta t_{\min}/T_{\text{rise}}$ were argued to be small, implying a narrow dispersion in Γ . We, however, find $\Delta t_{\min} \sim T_{\text{rise}}$, suggesting instead a broad range of possible Lorentz factors.

Finally, we find evidence that our minimum timescales correlate with redshift, possibly providing indication of cosmological time-dilation. However, the measurement threshold also appears to correlate strongly with redshift. This indicates that threshold effects likely dominate the apparent correlation and that the correlation may not be real. It is possible that additional features present in the

Haar scaleogram (slopes, breaks on longer timescales) – which richly describe the full GRB light curve and not just the minimum timescale – may yield correlations with intrinsic quantities like redshift. We will study this further in future work.

We thank Owen Littlejohns, Judd Bowman, and Teresa Ashcraft for comments on the manuscript and for useful discussions. We also thank our referee, Jay Norris, for insightful comments that improved the manuscript.

REFERENCES

- Abdo, A. A., Ackermann, M., Ajello, M., et al. 2010, ApJ, 722, 520
- Allan, D. W. 1966, Proceedings of the IEEE, 54, 221
- Aretxaga, I., Cid Fernandes, R., & Terlevich, R. J. 1997, MNRAS, 286, 271
- Beloborodov, A. M., Stern, B. E., & Svensson, R. 2000, ApJ, 535, 158
- Bhat, P. N. 2013, ArXiv e-prints, arXiv:1307.7618
- Bhat, P. N., Fishman, G. J., Meegan, C. A., et al. 1992, Nature, 359, 217
- Bhat, P. N., Briggs, M. S., Connaughton, V., et al. 2012, ApJ, 744, 141
- Bloom, J. S., Perley, D. A., Li, W., et al. 2009, ApJ, 691, 723
- Borgonovo, L. 2004, A&A, 418, 487
- Butler, N. 2013, The Astronomical Review, 8, 103
- Butler, N. R., Bloom, J. S., & Poznanski, D. 2010, ApJ, 711, 495
- Butler, N. R., Kocevski, D., Bloom, J. S., & Curtis, J. L. 2007, ApJ, 671, 656
- Cavallo, G., & Rees, M. J. 1978, MNRAS, 183, 359
- Chang, H.-Y. 2001, ApJ, 557, L85
- Chatfield, C. 2003, The analysis of time series: an introduction (CRC press)
- Chatterjee, R., Bailyn, C. D., Bonning, E. W., et al. 2012, ApJ, 749, 191
- Cristiani, S., Trentini, S., La Franca, F., et al. 1996, A&A, 306, 395
- Daubechies, I., ed. 1992, Ten lectures on wavelets
- Deng, M., & Schaefer, B. E. 1997, ApJ, 491, 720
- Dichiara, S., Guidorzi, C., Amati, L., & Frontera, F. 2013, MNRAS, 431, 3608
- Feigelson, E. D., & Nelson, P. I. 1985, ApJ, 293, 192
- Fenimore, E. E., Cooper, C., Ramirez-Ruiz, E., et al. 1999, ApJ, 512, 683
- Fenimore, E. E., in 't Zand, J. J. M., Norris, J. P., Bonnell, J. T., & Nemiroff, R. J. 1995, ApJ, 448, L101
- Fenimore, E. E., Madras, C. D., & Nayakshin, S. 1996, ApJ, 473, 998
- Gehrels, N., Chincarini, G., & Giommi, et al., P. 2004, ApJ, 611, 1005
- Guidorzi, C., Margutti, R., Amati, L., et al. 2012, MNRAS, 422, 1785
- Hawkins, M. R. S. 2002, MNRAS, 329, 76
- Hook, I. M., McMahon, R. G., Boyle, B. J., & Irwin, M. J. 1994, MNRAS, 268, 305
- Hughes, P. A., Aller, H. D., & Aller, M. F. 1992, ApJ, 396, 469
- in't Zand, J. J. M., & Fenimore, E. E. 1996, ApJ, 464, 622
- Kendall, M. G. 1938, Biometrika
- Kocevski, D., Butler, N., & Bloom, J. S. 2007, ApJ, 667, 1024
- Kocevski, D., & Petrosian, V. 2013, ApJ, 765, 116
- Kolaczyk, E. D. 1997, ApJ, 483, 340
- Link, B., Epstein, R. I., & Priedhorsky, W. C. 1993, ApJ, 408, L81
- Lloyd-Ronning, N. M., & Petrosian, V. 2002, ApJ, 565, 182
- MacLachlan, G. A., Shenoy, A., Sonbas, E., et al. 2013, MNRAS, 432, 857
- Mitrofanov, I. G. 1989, Ap&SS, 155, 141
- Nakar, E., & Piran, T. 2002, MNRAS, 330, 920
- Norris, J. P., Nemiroff, R. J., Bonnell, J. T., et al. 1996, ApJ, 459, 393
- Norris, J. P., Nemiroff, R. J., Scargle, J. D., et al. 1994, ApJ, 424, 540
- Norris, J. P., Scargle, J. D., & Bonnell, J. T. 2001, in Gamma-ray Bursts in the Afterglow Era, ed. E. Costa, F. Frontera, & J. Hjorth, 40
- Paczynski, B. 1986, ApJ, 308, L43
- Paltani, S. 1999, in Astronomical Society of the Pacific Conference Series, Vol. 159, BL Lac Phenomenon, ed. L. O. Takalo & A. Sillanpää, 293
- Percival, D. B., & Walden, A. T. 2006, Wavelet methods for time series analysis, Vol. 4 (Cambridge University Press)
- Piran, T. 2004, Reviews of Modern Physics, 76, 1143
- Quilligan, F., McBreen, B., Hanlon, L., et al. 2002, A&A, 385, 377
- Rees, M. J., & Meszaros, P. 1994, ApJ, 430, L93
- Reichart, D. E., et al. 2001, ApJ, 552, 57
- Scargle, J. D., Norris, J. P., Jackson, B., & Chiang, J. 2013, ApJ, 764, 167
- Schaefer, B. E., Cohen, J., Teegarden, B. J., et al. 1993, ApJ, 404, 673
- Simonetti, J. H., Cordes, J. M., & Heeschen, D. S. 1985, ApJ, 296, 46
- Trevese, D., Kron, R. G., Majewski, S. R., Bershadsky, M. A., & Koo, D. C. 1994, ApJ, 433, 494
- Walker, K. C., Schaefer, B. E., & Fenimore, E. E. 2000, ApJ, 537, 264
- Wyithe, J. S. B., & Turner, E. L. 2001, MNRAS, 320, 21
- Zhang, F.-W., Fan, Y.-Z., Shao, L., & Wei, D.-M. 2013, ApJ, 778, L11

TABLE 1 GRB Minimum Timescales

GRB	Δt_{\min} [s]	Δt_{snr} [s]	T_{90} [s]	T_{R45} [s]	$\sigma_{X,t_{\min}}$	$\sigma_{X,t_{\text{snr}}}$	χ^2/ν	S/N	z
041220	1.78 ± 0.30	0.64 ± 0.11	3.52 ± 0.13	1.04 ± 0.054	0.468	0.249	0.0005	23.5	...
041223	0.32 ± 0.05	0.12 ± 0.02	108.00 ± 0.52	19.2 ± 0.22	0.255	0.118	1.119	177.1	...
041224	2.51 ± 0.43	1.00 ± 0.48	141.48 ± 1.89	27.54 ± 0.71	0.253	0.134	1.099	54.9	...
041228	9.90 ± 1.68	3.54 ± 0.60	55.50 ± 3.39	16.28 ± 0.442	0.302	0.155	0.478	42.2	...
050117	...	0.31 ± 0.22	168.96 ± 0.86	47.52 ± 0.854	...	0.179	9.758	78.4	...
050124	0.64 ± 0.11	0.23 ± 0.14	3.36 ± 0.13	1.08 ± 0.033	0.359	0.190	2.067	36.9	...
050128	...	0.18 ± 0.09	24.48 ± 3.63	4.48 ± 0.187	...	0.297	3.583	41.6	...
050215A	...	5.58 ± 2.64	66.50 ± 0.99	6 ± 0.429	...	0.621	3.452	10.2	...
050219A	3.54 ± 0.60	1.31 ± 0.78	25.00 ± 1.04	8.25 ± 0.226	0.358	0.141	0.063	50.8	...
050219B	...	0.18 ± 0.09	20.93 ± 0.92	4.81 ± 0.097	...	0.179	2.794	71.9	...
050306	3.54 ± 0.60	1.31 ± 0.78	112.66 ± 1.37	36.68 ± 0.886	0.404	0.226	2.353	26.5	...
050315	...	0.79 ± 0.26	94.60 ± 1.66	19.25 ± 0.53	...	0.214	13.989	43.7	1.949
050318	0.64 ± 0.11	0.23 ± 0.14	30.96 ± 0.09	3.52 ± 0.128	0.383	0.176	0.345	49	1.44
050319	4.99 ± 0.85	1.73 ± 1.20	153.55 ± 2.20	11.84 ± 0.956	0.727	0.355	1.734	18.2	3.24
050326	0.23 ± 0.04	0.12 ± 0.02	30.24 ± 0.44	5.67 ± 0.08	0.210	0.122	0.457	132.7	...
050401	2.51 ± 0.43	0.79 ± 0.26	34.41 ± 0.34	5.18 ± 0.212	0.534	0.210	0.056	39.3	2.9
050410	...	19.66 ± 3.34	45.08 ± 2.94	17.48 ± 0.607	...	0.221	8.085	36.2	...
050416A	1.26 ± 0.21	0.64 ± 0.11	2.91 ± 0.18	0.63 ± 0.043	0.851	0.653	2.398	17.5	0.6535
050416B	1.78 ± 0.30	0.64 ± 0.11	3.32 ± 0.19	0.88 ± 0.051	0.561	0.338	0.089	19.9	...
050418	2.51 ± 0.43	0.79 ± 0.26	82.77 ± 0.56	14.24 ± 0.475	0.375	0.130	0.174	46.1	...
050422	13.95 ± 2.37	5.58 ± 2.64	59.52 ± 0.74	6.88 ± 0.425	0.604	0.422	1.812	14	...
050502B	2.51 ± 0.43	0.64 ± 0.11	17.44 ± 0.26	2.12 ± 0.111	0.663	0.239	0.755	25.3	...
050505	...	3.54 ± 0.60	60.20 ± 1.35	9.6 ± 0.432	...	0.378	5.948	21.8	4.27
050509A	4.99 ± 0.85	1.73 ± 1.20	11.76 ± 0.90	2.8 ± 0.148	0.429	0.232	0.759	23.3	...
050525	0.12 ± 0.02	0.03 ± 0.02	9.10 ± 0.04	2.6 ± 0.038	0.130	0.045	0.021	339.9	0.606
050603	0.23 ± 0.04	0.12 ± 0.02	9.80 ± 0.39	1.6 ± 0.08	0.531	0.319	0.827	42	2.821
050607	3.54 ± 0.60	1.31 ± 0.78	17.29 ± 0.47	4.37 ± 0.222	0.607	0.313	0.305	14.7	...
050701	1.26 ± 0.21	0.64 ± 0.11	32.24 ± 1.39	4.81 ± 0.172	0.477	0.292	0.614	40.8	...
050713A	...	0.79 ± 0.26	124.65 ± 13.10	7.65 ± 0.208	...	0.110	2.944	72.8	...
050713B	39.04 ± 6.63	9.63 ± 6.69	132.94 ± 5.84	23.12 ± 1.621	1.159	0.345	0.047	14.3	...
050715	...	1.31 ± 0.78	185.35 ± 5.64	21.45 ± 1.346	...	0.321	2.985	28.7	...
050716	9.90 ± 1.68	3.54 ± 0.60	64.24 ± 0.91	22.88 ± 0.636	0.399	0.182	0.028	20.7	...
050717	...	0.12 ± 0.02	79.38 ± 2.23	11.34 ± 0.278	...	0.197	5.133	80.7	...
050721	9.90 ± 1.68	4.39 ± 1.45	39.56 ± 1.97	9.03 ± 0.592	0.802	0.468	2.448	16.4	...
050724	0.23 ± 0.04	0.12 ± 0.02	2.50 ± 0.04	0.24 ± 0.022	0.858	0.555	1.12	20.8	0.258
050726	...	30.99 ± 14.67	191.49 ± 2.27	12.09 ± 1.182	...	0.528	17.183	14.3	...
050730	...	19.66 ± 3.34	60.48 ± 2.26	20.79 ± 1.217	...	0.288	4.281	13.2	3.969
050801	1.78 ± 0.30	0.79 ± 0.26	5.88 ± 0.20	1 ± 0.067	0.796	0.443	0.388	18.2	1.56
050803	...	3.54 ± 0.60	88.20 ± 1.35	16.8 ± 0.796	...	0.346	7.235	19.9	0.422
050820A	...	1.00 ± 0.48	239.68 ± 0.37	11.04 ± 0.486	...	0.158	6.907	41.4	2.6147
050820B	0.45 ± 0.08	0.18 ± 0.09	12.69 ± 0.21	3.15 ± 0.057	0.176	0.100	1.988	80.7	...
050822	2.51 ± 0.43	0.79 ± 0.26	104.88 ± 2.63	15.87 ± 0.63	0.432	0.228	0.326	31.7	1.434
050827	...	0.79 ± 0.26	50.16 ± 2.19	7.41 ± 0.371	...	0.200	18.603	35.8	...
050904	...	9.63 ± 6.69	197.20 ± 2.26	70.72 ± 1.588	...	0.114	3.09	38.4	6.29
050911	3.54 ± 0.60	1.31 ± 0.78	16.29 ± 0.13	1.05 ± 0.107	0.884	0.658	0.033	10.4	...
050915A	...	1.31 ± 0.78	21.39 ± 0.59	5.06 ± 0.26	...	0.474	8.993	12.6	2.5273
050915B	...	1.00 ± 0.48	41.20 ± 1.21	15.6 ± 0.301	...	0.145	10.202	60.6	...
050922B	...	19.66 ± 3.34	251.72 ± 22.34	11.9 ± 0.868	...	0.670	4.557	14.6	...
050922C	...	0.12 ± 0.02	4.56 ± 0.12	1.2 ± 0.027	...	0.158	3.384	60	2.198
051001	...	19.66 ± 3.34	55.90 ± 1.63	19.5 ± 0.705	...	0.259	3.014	21.1	2.4296
051006	...	0.64 ± 0.11	26.46 ± 0.53	3.92 ± 0.28	...	0.610	2.796	17.3	1.059
051008	...	0.64 ± 0.11	45.10 ± 1.02	8.58 ± 0.26	...	0.207	7.985	62.1	...
051021B	9.90 ± 1.68	4.39 ± 1.45	33.54 ± 1.37	8.06 ± 0.435	0.667	0.338	0.151	18.8	...
051111	...	0.64 ± 0.11	50.96 ± 2.45	9.88 ± 0.23	...	0.145	5.237	62.6	1.55
051113	...	1.00 ± 0.48	96.75 ± 0.80	15.05 ± 0.821	...	0.394	9.862	19.4	...
051117A	27.70 ± 4.70	9.63 ± 6.69	238.14 ± 13.14	58.32 ± 1.415	0.297	0.110	0.091	53.8	...
051221A	0.01 ± 0.001	0.005 ± 0.001	1.24 ± 0.03	0.16 ± 0.008	0.383	0.219	0.196	65.6	0.5459
051227	...	1.00 ± 0.48	4.30 ± 0.19	0.85 ± 0.076	...	0.482	2.809	12.5	0.714

Continued on Next Page...

TABLE 1 – Continued

GRB	Δt_{\min}	Δt_{snr}	T_{90}	T_{R45}	$\sigma_{X,t_{\min}}$	$\sigma_{X,t_{\text{snr}}}$	χ^2/ν	S/N	z
060102	...	0.06 ± 0.04	3.76 ± 0.36	0.84 ± 0.074	...	0.876	10.871	8.6	...
060105	...	0.14 ± 0.05	55.20 ± 0.34	13.8 ± 0.148	...	0.126	5.052	134.4	...
060108	7.03 ± 1.19	3.54 ± 0.60	15.28 ± 1.10	3.36 ± 0.176	0.581	0.429	0.248	20.5	2.03
060110	...	0.79 ± 0.26	24.00 ± 1.19	5.64 ± 0.146	...	0.114	2.915	51.7	...
060111A	...	1.00 ± 0.48	15.26 ± 0.89	4.9 ± 0.131	...	0.118	2.841	49.2	...
060111B	...	1.73 ± 1.20	61.38 ± 1.22	10.56 ± 0.674	...	0.386	3.821	19.8	...
060115	...	3.54 ± 0.60	109.89 ± 1.14	15.66 ± 0.687	...	0.319	3.464	27.4	3.53
060117	0.12 ± 0.02	0.03 ± 0.02	17.29 ± 0.11	3.61 ± 0.073	0.224	0.071	0.165	186.7	...
060202	...	19.66 ± 3.34	205.92 ± 2.52	58.5 ± 2.272	...	0.415	11.538	15.1	0.783
060204B	...	1.31 ± 0.78	40.68 ± 1.40	12.96 ± 0.306	...	0.155	6.533	43.2	...
060206	1.26 ± 0.21	0.64 ± 0.11	6.06 ± 0.16	1.92 ± 0.048	0.385	0.212	0.104	45.1	4.045
060210	1.26 ± 0.21	0.64 ± 0.11	369.94 ± 20.65	35.51 ± 1.555	0.336	0.292	1.471	42.8	3.91
060211B	...	3.54 ± 0.60	11.13 ± 0.57	2.73 ± 0.231	...	0.723	8.384	11.9	...
060223A	4.99 ± 0.85	1.73 ± 1.20	8.40 ± 0.28	2.6 ± 0.128	0.351	0.200	0.004	18	4.41
060223B	...	0.18 ± 0.09	10.60 ± 0.28	3.7 ± 0.094	...	0.197	5.135	52.2	...
060306	...	0.14 ± 0.05	60.96 ± 0.80	3.64 ± 0.202	...	0.249	3.321	42.5	3.5
060312	2.51 ± 0.43	1.00 ± 0.48	45.25 ± 0.86	12 ± 0.324	0.239	0.152	2.277	42.9	...
060313	...	0.02 ± 0.002	0.78 ± 0.01	0.18 ± 0.008	...	0.346	8.479	48.4	...
060319	...	0.79 ± 0.26	5.28 ± 0.28	1.56 ± 0.112	...	0.471	5.361	13.2	...
060322	...	0.79 ± 0.26	210.40 ± 1.04	21.6 ± 0.688	...	0.141	5.938	51.1	...
060403	7.03 ± 1.19	3.54 ± 0.60	26.40 ± 0.57	8.1 ± 0.29	0.608	0.329	0.16	22.2	...
060413	7.03 ± 1.19	3.54 ± 0.60	120.84 ± 3.89	29.64 ± 0.693	0.197	0.114	0.006	58.4	...
060418	...	0.14 ± 0.05	103.24 ± 10.33	14.5 ± 0.297	...	0.200	7.018	80.6	1.489
060421	...	0.64 ± 0.11	11.11 ± 0.46	2.53 ± 0.068	...	0.176	3.918	42.1	...
060424	...	0.64 ± 0.11	37.86 ± 0.50	3.54 ± 0.219	...	0.706	5.333	14.9	...
060428A	2.51 ± 0.43	0.79 ± 0.26	52.60 ± 3.38	7.4 ± 0.271	0.454	0.164	0.011	37.9	...
060501	2.51 ± 0.43	1.00 ± 0.48	12.18 ± 0.42	3.78 ± 0.16	0.525	0.326	2.67	22.3	...
060502A	13.95 ± 2.37	3.54 ± 0.60	30.24 ± 4.18	8.61 ± 0.241	0.481	0.158	0.021	45.7	1.51
060502B	0.08 ± 0.01	0.03 ± 0.01	0.16 ± 0.02	0.04 ± 0.007	0.933	0.607	0.274	13	0.287
060507	...	3.54 ± 0.60	52.08 ± 1.43	17.36 ± 0.754	...	0.402	8.001	15.7	...
060510A	2.51 ± 0.43	1.00 ± 0.48	21.85 ± 0.77	4.37 ± 0.221	0.541	0.295	1.864	27.8	...
060510B	...	1.99 ± 0.94	229.89 ± 2.77	78.57 ± 2.077	...	0.315	50.089	22.3	4.9
060515	...	19.66 ± 3.34	59.85 ± 3.67	13.68 ± 0.851	...	0.488	4.495	17.3	...
060526	1.78 ± 0.30	0.79 ± 0.26	295.55 ± 4.01	13.57 ± 1.063	0.421	0.348	2.173	23.5	3.221
060607A	7.03 ± 1.19	1.31 ± 0.78	102.55 ± 3.35	15.05 ± 0.537	0.496	0.118	0.198	50.7	3.082
060607B	...	3.54 ± 0.60	31.03 ± 1.54	8.41 ± 0.39	...	0.319	7.49	25.8	...
060614	...	0.12 ± 0.02	108.80 ± 0.86	27.2 ± 0.375	...	0.100	2.946	191.9	0.125
060707	13.95 ± 2.37	5.58 ± 2.64	75.14 ± 2.46	14.3 ± 0.676	0.539	0.310	1.413	20.1	3.425
060708	...	0.64 ± 0.11	7.50 ± 0.45	1.86 ± 0.081	...	0.342	6.693	30.1	1.92
060714	...	1.00 ± 0.48	118.72 ± 1.87	22.08 ± 0.767	...	0.212	7.126	44	2.711
060719	1.78 ± 0.30	0.79 ± 0.26	57.00 ± 0.84	5.8 ± 0.24	0.219	0.138	2.216	47.2	1.532
060729	4.99 ± 0.85	1.73 ± 1.20	119.14 ± 1.40	18.13 ± 0.794	0.356	0.161	0.182	44.9	0.54
060813	...	0.14 ± 0.05	15.84 ± 0.74	3.42 ± 0.057	...	0.105	7.665	101.9	...
060814	0.90 ± 0.15	0.31 ± 0.22	159.16 ± 4.08	25.76 ± 0.458	0.152	0.063	0.641	173.9	0.84
060825	1.26 ± 0.21	0.64 ± 0.11	8.55 ± 0.23	2.97 ± 0.079	0.355	0.243	1.355	47.3	...
060904A	0.23 ± 0.04	0.12 ± 0.02	75.21 ± 0.57	14.03 ± 0.204	0.176	0.114	0.704	127.1	...
060904B	...	1.00 ± 0.48	171.04 ± 2.29	5.92 ± 0.401	...	0.158	3.506	34.2	0.703
060906	2.51 ± 0.43	1.00 ± 0.48	72.96 ± 9.41	12.48 ± 0.618	0.362	0.274	0.613	30.5	3.686
060908	...	0.64 ± 0.11	18.48 ± 0.17	5.28 ± 0.119	...	0.192	6.975	47.4	1.8836
060912A	0.64 ± 0.11	0.23 ± 0.14	5.92 ± 0.35	1.12 ± 0.037	0.407	0.138	0.0005	43.5	0.937
060919	2.51 ± 0.43	1.00 ± 0.48	4.70 ± 0.17	1.25 ± 0.078	0.546	0.344	0.0005	17.2	...
060923A	...	5.58 ± 2.64	56.98 ± 2.49	5.18 ± 0.47	...	0.655	23.112	10.6	...
060926	3.54 ± 0.60	1.31 ± 0.78	7.05 ± 0.39	1.5 ± 0.089	0.456	0.303	1.435	17	3.2
060927	1.26 ± 0.21	0.31 ± 0.22	23.03 ± 0.26	3.22 ± 0.13	0.502	0.155	0.091	43.1	5.6
060929	...	19.66 ± 3.34	550.44 ± 2.05	14.22 ± 1.422	...	1.075	5.722	11	...
061004	1.26 ± 0.21	0.31 ± 0.22	6.54 ± 0.23	1.62 ± 0.059	0.574	0.145	0.097	37.5	...
061006	0.08 ± 0.01	0.03 ± 0.02	1.54 ± 0.09	0.24 ± 0.01	0.409	0.219	1.802	42.6	...
061007	0.16 ± 0.03	0.06 ± 0.04	74.90 ± 0.51	16.8 ± 0.122	0.118	0.045	0.005	330.4	1.261
061021	0.64 ± 0.11	0.23 ± 0.14	12.06 ± 0.32	2.52 ± 0.069	0.298	0.118	0.304	50.9	0.3463

Continued on Next Page...

TABLE 1 – Continued

GRB	Δt_{\min}	Δt_{snr}	T_{90}	T_{R45}	$\sigma_{X,t_{\min}}$	$\sigma_{X,t_{\text{snr}}}$	χ^2/ν	S/N	z
061110A	19.66 ± 3.34	7.26 ± 4.32	47.04 ± 1.80	14.88 ± 0.635	0.383	0.187	0.008	24.1	0.757
061121	0.12 ± 0.02	0.04 ± 0.03	83.00 ± 12.50	5.8 ± 0.06	0.130	0.055	0.52	273.8	1.314
061126	0.23 ± 0.04	0.12 ± 0.02	26.78 ± 0.46	5.46 ± 0.134	0.176	0.134	1.349	85.7	1.159
061201	...	0.12 ± 0.02	0.86 ± 0.03	0.22 ± 0.014	...	0.456	3.274	21.4	...
061202	1.26 ± 0.21	0.64 ± 0.11	125.35 ± 17.30	12.19 ± 0.312	0.184	0.110	0.401	85.5	...
061210	...	0.01 ± 0.01	0.10 ± 0.01	0.04 ± 0.009	...	0.375	7.051	22.5	0.41
061222A	0.12 ± 0.02	0.04 ± 0.03	81.65 ± 4.24	8.97 ± 0.159	0.200	0.089	0.489	139.9	2.088
061222B	...	5.58 ± 2.64	42.00 ± 2.15	12.4 ± 0.56	...	0.297	24.964	22.6	3.355
070103	...	0.64 ± 0.11	10.92 ± 0.14	1.47 ± 0.157	...	0.773	7.521	9.1	2.6208
070107	...	1.31 ± 0.78	357.50 ± 9.40	22.55 ± 0.99	...	0.145	9.529	48.2	...
070110	...	5.58 ± 2.64	47.70 ± 1.54	16.2 ± 0.572	...	0.210	6.48	25.9	2.352
070129	...	4.39 ± 1.45	92.15 ± 2.24	27.55 ± 0.979	...	0.348	5.09	22.2	2.3384
070220	0.45 ± 0.08	0.18 ± 0.09	150.67 ± 7.75	18.3 ± 0.361	0.197	0.105	0.944	114.6	...
070223	9.90 ± 1.68	4.39 ± 1.45	76.32 ± 1.66	21.2 ± 0.955	0.510	0.329	0.919	14.6	...
070306	1.26 ± 0.21	0.64 ± 0.11	261.36 ± 6.65	16.02 ± 0.753	0.232	0.141	2.017	85.4	1.497
070318	4.99 ± 0.85	1.00 ± 0.48	51.00 ± 2.32	10.25 ± 0.336	0.391	0.114	1.27	48.1	0.836
070328	0.90 ± 0.15	0.31 ± 0.22	49.60 ± 1.11	12.71 ± 0.156	0.182	0.089	1.232	110.4	...
070411	...	1.31 ± 0.78	108.56 ± 3.62	31.86 ± 1.417	...	0.228	24.981	30.4	2.954
070419B	4.99 ± 0.85	1.73 ± 1.20	133.75 ± 2.85	41.25 ± 0.576	0.251	0.095	0.247	84.6	...
070420	...	1.00 ± 0.48	95.91 ± 1.64	22.24 ± 0.718	...	0.148	5.253	63.7	...
070427	...	0.79 ± 0.26	12.24 ± 0.44	4.32 ± 0.121	...	0.190	7.941	40	...
070508	0.08 ± 0.01	0.03 ± 0.01	21.20 ± 0.25	5.2 ± 0.02	0.161	0.063	0.142	262.1	0.82
070517	2.51 ± 0.43	1.00 ± 0.48	6.16 ± 0.27	1.47 ± 0.094	0.893	0.636	1.603	8.7	...
070521	0.23 ± 0.04	0.12 ± 0.02	561.20 ± 6.66	10.58 ± 0.341	0.268	0.161	0.474	118.6	...
070529	19.66 ± 3.34	5.58 ± 2.64	112.21 ± 2.94	22.9 ± 1.595	0.819	0.434	2.329	13.5	2.4996
070531	13.95 ± 2.37	5.58 ± 2.64	37.20 ± 3.01	6.6 ± 0.441	0.608	0.407	0.87	14.4	...
070612A	27.70 ± 4.70	9.63 ± 6.69	254.74 ± 3.63	62.33 ± 2.175	0.514	0.179	1.147	24.9	0.617
070612B	4.99 ± 0.85	1.73 ± 1.20	15.52 ± 1.09	4.32 ± 0.204	0.577	0.245	0.482	24.2	...
070616	1.26 ± 0.21	0.64 ± 0.11	443.52 ± 9.13	134.64 ± 1.813	0.170	0.114	0.863	149.2	...
070621	...	0.79 ± 0.26	36.12 ± 0.81	13.02 ± 0.294	...	0.200	3.027	48.8	...
070628	2.51 ± 0.43	1.00 ± 0.48	13.26 ± 0.39	4.42 ± 0.097	0.268	0.118	0.104	50.5	...
070704	1.26 ± 0.21	0.64 ± 0.11	384.78 ± 4.64	31.35 ± 0.921	0.230	0.134	0.005	74.2	...
070714A	1.26 ± 0.21	0.64 ± 0.11	2.56 ± 0.24	0.62 ± 0.033	0.582	0.500	2.673	21.5	...
070714B	0.12 ± 0.02	0.04 ± 0.03	64.18 ± 1.60	1.4 ± 0.132	0.679	0.339	0.662	35.8	0.92
070721B	...	0.79 ± 0.26	330.66 ± 6.28	16.72 ± 0.813	...	0.293	5.287	26.8	3.626
070808	3.54 ± 0.60	1.00 ± 0.48	57.20 ± 4.87	5.28 ± 0.256	0.753	0.247	0.249	24.3	...
070810A	...	1.73 ± 1.20	7.68 ± 0.41	2.48 ± 0.109	...	0.228	4.068	24.6	2.17
070911	0.45 ± 0.08	0.18 ± 0.09	177.00 ± 2.69	40.12 ± 0.611	0.214	0.105	0.588	148.6	...
070917	0.64 ± 0.11	0.14 ± 0.05	7.44 ± 0.39	1.52 ± 0.028	0.263	0.089	2.213	82	...
070920A	27.70 ± 4.70	10.23 ± 6.09	57.00 ± 1.50	13.8 ± 0.867	0.831	0.529	2.149	12.9	...
070920B	9.90 ± 1.68	3.54 ± 0.60	21.63 ± 0.59	7.14 ± 0.261	0.451	0.200	0.0005	31.3	...
071001	7.03 ± 1.19	3.54 ± 0.60	66.30 ± 1.87	7.8 ± 0.406	0.647	0.468	2.499	20.1	...
071003	...	0.18 ± 0.09	148.32 ± 0.68	10.32 ± 0.276	...	0.148	4.527	79.7	1.605
071010B	0.90 ± 0.15	0.31 ± 0.22	34.68 ± 1.02	4.68 ± 0.075	0.155	0.055	0.624	136.3	0.947
071011	3.54 ± 0.60	1.31 ± 0.78	87.04 ± 5.23	18.36 ± 0.937	0.643	0.297	0.02	28.7	...
071020	...	0.04 ± 0.03	4.40 ± 0.27	1.36 ± 0.021	...	0.126	5.084	100.3	2.145
071021	13.95 ± 2.37	5.58 ± 2.64	204.96 ± 17.95	18.48 ± 1.155	0.567	0.333	0.197	17.7	2.452
071025	2.51 ± 0.43	1.00 ± 0.48	161.17 ± 5.40	39.05 ± 0.641	0.202	0.114	1.575	86	...
071031	19.66 ± 3.34	5.58 ± 2.64	187.18 ± 7.12	34.38 ± 2.665	0.911	0.470	1.221	15.9	2.692
071117	0.64 ± 0.11	0.18 ± 0.09	6.48 ± 0.76	1.28 ± 0.03	0.315	0.095	0.071	76.4	1.331
071129	27.70 ± 4.70	9.63 ± 6.69	206.08 ± 6.98	27.2 ± 1.237	0.717	0.270	2.21	23.9	...
080205	9.90 ± 1.68	3.54 ± 0.60	113.27 ± 2.65	20.68 ± 0.866	0.526	0.266	0.209	33.6	...
080207	...	1.31 ± 0.78	310.98 ± 9.34	71.54 ± 6.686	...	0.217	9.354	61.9	2.0858
080210	...	3.54 ± 0.60	43.89 ± 4.36	8.82 ± 0.364	...	0.274	13.123	36.6	2.641
080212	...	5.58 ± 2.64	132.24 ± 2.55	34.96 ± 1.356	...	0.279	4.293	24.7	...
080229A	0.23 ± 0.04	0.12 ± 0.02	50.18 ± 1.47	7.02 ± 0.13	0.205	0.122	0.322	111.6	...
080303	4.99 ± 0.85	1.31 ± 0.78	44.68 ± 2.41	2.68 ± 0.199	0.944	0.371	0.002	17.5	...
080307	...	24.36 ± 8.04	97.82 ± 5.26	18.76 ± 1.275	...	0.464	5.109	16.9	...
080310	19.66 ± 3.34	5.58 ± 2.64	361.92 ± 3.75	23.68 ± 1.051	0.559	0.192	0.005	27.5	2.4266

Continued on Next Page...

TABLE 1 – Continued

GRB	Δt_{\min}	Δt_{snr}	T_{90}	T_{R45}	$\sigma_{X,t_{\min}}$	$\sigma_{X,t_{\text{snr}}}$	χ^2/ν	S/N	z
080319A	...	5.58 ± 2.64	45.63 ± 1.62	13.26 ± 0.533	...	0.308	6.849	23.9	...
080319B	0.04 ± 0.01	0.02 ± 0.002	147.32 ± 2.50	20.3 ± 0.058	0.063	0.032	0.212	725.4	0.937
080319C	1.78 ± 0.30	0.79 ± 0.26	32.88 ± 3.27	5.04 ± 0.152	0.277	0.155	0.038	60.5	1.95
080320	9.90 ± 1.68	3.54 ± 0.60	21.42 ± 2.10	4.14 ± 0.329	0.685	0.598	0.495	13.6	...
080325	109.21 ± 18.55	40.33 ± 24.01	183.92 ± 5.98	41.14 ± 2.695	0.757	0.421	0.026	18.1	...
080328	0.45 ± 0.08	0.18 ± 0.09	91.00 ± 0.30	16 ± 0.174	0.173	0.114	2.235	83.7	...
080330	...	9.63 ± 6.69	66.10 ± 0.98	4 ± 0.358	...	0.531	7.587	13.4	1.51
080409	1.26 ± 0.21	0.64 ± 0.11	9.94 ± 0.12	0.9 ± 0.054	0.631	0.457	1.804	24.7	...
080411	0.16 ± 0.03	0.04 ± 0.03	58.29 ± 0.46	6.7 ± 0.067	0.114	0.032	1.085	379.3	1.03
080413A	0.64 ± 0.11	0.23 ± 0.14	46.62 ± 0.13	5.25 ± 0.143	0.210	0.089	0.147	74.8	2.433
080413B	0.45 ± 0.08	0.18 ± 0.09	7.04 ± 0.43	1.16 ± 0.032	0.326	0.130	1.271	64.4	1.1
080426	0.32 ± 0.05	0.12 ± 0.02	1.72 ± 0.10	0.34 ± 0.019	0.695	0.279	0.064	28.1	...
080430	2.51 ± 0.43	0.64 ± 0.11	16.20 ± 0.78	3.42 ± 0.084	0.484	0.145	1.89	52.7	0.767
080503	...	1.73 ± 1.20	178.92 ± 19.16	27.09 ± 1.534	...	0.261	5.171	34.5	...
080515	9.90 ± 1.68	3.54 ± 0.60	22.05 ± 1.34	6.09 ± 0.296	0.675	0.401	0.644	18.8	...
080516	...	0.64 ± 0.11	6.84 ± 0.17	0.99 ± 0.104	...	0.851	11.739	11.9	...
080520	...	0.23 ± 0.14	2.97 ± 0.24	0.51 ± 0.051	...	1.171	4.533	8.3	1.545
080523	19.66 ± 3.34	7.26 ± 4.32	55.38 ± 3.25	12.87 ± 0.713	0.571	0.305	0.041	21.6	...
080602	...	0.31 ± 0.22	85.12 ± 2.65	7 ± 0.313	...	0.214	3.884	39.5	...
080603B	0.23 ± 0.04	0.12 ± 0.02	59.50 ± 0.51	6.16 ± 0.152	0.195	0.164	1.087	70	2.69
080605	...	0.12 ± 0.02	19.57 ± 0.32	4.75 ± 0.079	...	0.138	8.338	157.5	1.6398
080607	0.32 ± 0.05	0.14 ± 0.05	83.66 ± 0.83	7.52 ± 0.094	0.247	0.145	0.796	123	3.036
080613B	0.23 ± 0.04	0.12 ± 0.02	83.21 ± 5.07	15.9 ± 0.356	0.313	0.217	0.783	94.4	...
080623	...	1.31 ± 0.78	16.10 ± 1.11	2.9 ± 0.158	...	0.316	7.376	21.5	...
080701	3.54 ± 0.60	1.00 ± 0.48	9.35 ± 0.49	2.3 ± 0.098	0.574	0.190	0.137	26.7	...
080707	...	3.54 ± 0.60	30.25 ± 0.43	3.3 ± 0.189	...	0.546	15.939	17.2	1.23
080714	1.78 ± 0.30	0.64 ± 0.11	34.20 ± 2.29	4.7 ± 0.208	0.406	0.184	0.085	44.9	...
080721	1.26 ± 0.21	0.64 ± 0.11	29.92 ± 2.29	4.51 ± 0.195	0.467	0.295	1.324	37.2	2.602
080723A	...	1.73 ± 1.20	24.89 ± 2.81	3.8 ± 0.34	...	0.509	3.905	14	...
080725	4.99 ± 0.85	1.73 ± 1.20	129.64 ± 4.42	11.2 ± 0.541	0.324	0.130	0.046	46.1	...
080727B	...	0.12 ± 0.02	18.30 ± 10.97	2.2 ± 0.058	...	0.192	20.44	81.4	...
080727C	1.78 ± 0.30	0.79 ± 0.26	99.84 ± 5.99	18.24 ± 0.427	0.247	0.134	1.115	76.2	...
080802	...	19.66 ± 3.34	173.60 ± 9.01	30.24 ± 1.923	...	0.580	4.468	18	...
080804	...	4.39 ± 1.45	61.74 ± 8.81	7.92 ± 0.342	...	0.200	7.444	31.1	2.2
080805	13.95 ± 2.37	3.54 ± 0.60	111.84 ± 9.11	19.68 ± 0.683	0.483	0.141	1.828	49.7	1.505
080810	...	0.64 ± 0.11	453.15 ± 5.09	31.35 ± 1.229	...	0.265	7.042	57.9	3.35
080903	...	1.73 ± 1.20	69.30 ± 3.38	15.51 ± 0.587	...	0.200	15.485	37.5	...
080905A	0.45 ± 0.08	0.18 ± 0.09	1.04 ± 0.03	0.18 ± 0.019	0.671	0.685	2.466	11.4	0.1218
080905B	4.99 ± 0.85	1.73 ± 1.20	103.97 ± 4.68	13.32 ± 0.845	0.543	0.310	2.201	22.8	2.374
080906	...	7.26 ± 4.32	159.28 ± 6.95	29.92 ± 1.164	...	0.145	8.826	47.2	...
080915B	0.45 ± 0.08	0.18 ± 0.09	3.64 ± 0.24	0.84 ± 0.019	0.322	0.141	1.021	53.3	...
080916A	...	0.64 ± 0.11	62.53 ± 3.24	13.32 ± 0.273	...	0.100	3.07	89.3	0.689
080928	...	0.64 ± 0.11	284.90 ± 12.16	23.38 ± 0.935	...	0.374	3.327	39.8	1.692
081007	3.54 ± 0.60	1.31 ± 0.78	5.55 ± 0.26	1.6 ± 0.082	0.422	0.339	1.64	19.6	0.5295
081008	...	0.79 ± 0.26	199.32 ± 11.52	31.71 ± 0.844	...	0.173	4.481	50.7	1.9685
081012	...	4.39 ± 1.45	32.00 ± 2.32	6 ± 0.398	...	0.552	5.651	16.3	...
081022	...	19.66 ± 3.34	149.60 ± 8.46	42.9 ± 1.649	...	0.361	5.614	28.3	...
081024A	...	0.18 ± 0.09	1.86 ± 0.05	0.26 ± 0.024	...	0.537	3.939	14.5	...
081028	55.00 ± 9.34	19.66 ± 3.34	275.59 ± 9.68	78.12 ± 2.09	0.485	0.224	0.139	42	3.038
081102	7.03 ± 1.19	3.54 ± 0.60	63.00 ± 4.72	13.05 ± 0.663	0.559	0.319	0.096	25.4	...
081104	27.70 ± 4.70	9.63 ± 6.69	41.36 ± 1.21	13.2 ± 0.609	0.327	0.251	0.964	22.4	...
081109A	9.90 ± 1.68	3.54 ± 0.60	70.14 ± 1.89	17.22 ± 0.417	0.342	0.122	0.097	58.7	...
081118	39.04 ± 6.63	15.61 ± 7.39	66.55 ± 5.08	18.15 ± 0.877	0.481	0.270	0.141	19.8	2.58
081126	...	0.64 ± 0.11	59.60 ± 1.40	6.55 ± 0.193	...	0.219	13.958	52.9	...
081128	...	0.79 ± 0.26	108.48 ± 3.63	24 ± 0.939	...	0.297	45.3	36.2	...
081203A	...	0.31 ± 0.22	254.28 ± 26.94	31.2 ± 0.825	...	0.173	6.359	80.3	2.1
081210	...	0.23 ± 0.14	150.97 ± 1.85	11.78 ± 0.655	...	0.221	10.995	35.9	...
081221	0.64 ± 0.11	0.18 ± 0.09	34.23 ± 0.64	7.98 ± 0.086	0.126	0.032	1.137	278.7	2.26
081222	0.45 ± 0.08	0.14 ± 0.05	33.48 ± 1.44	4.2 ± 0.053	0.158	0.063	0.026	147.6	2.77

Continued on Next Page...

TABLE 1 – Continued

GRB	Δt_{\min}	Δt_{snr}	T_{90}	T_{R45}	$\sigma_{X,t_{\min}}$	$\sigma_{X,t_{\text{snr}}}$	χ^2/ν	S/N	z
081230	...	5.15 ± 3.07	55.10 ± 1.25	11.78 ± 0.66	...	0.283	4.571	22.2	...
090102	...	0.79 ± 0.26	30.69 ± 1.21	8.25 ± 0.297	...	0.277	4.99	35.5	1.547
090113	0.64 ± 0.11	0.23 ± 0.14	8.80 ± 0.13	2 ± 0.088	0.545	0.257	0.393	32.3	1.7493
090123	13.95 ± 2.37	4.39 ± 1.45	141.96 ± 5.23	25.35 ± 1.69	0.646	0.285	1.702	24.6	...
090129	2.51 ± 0.43	0.79 ± 0.26	18.20 ± 0.91	4.55 ± 0.111	0.341	0.110	0.064	68.7	...
090201	...	0.64 ± 0.11	89.44 ± 1.72	16.34 ± 0.463	...	0.148	4.291	88.6	...
090301	0.23 ± 0.04	0.12 ± 0.02	42.64 ± 1.25	10.66 ± 0.173	0.158	0.089	0.015	179.8	...
090313	...	3.54 ± 0.60	90.24 ± 6.75	22.56 ± 1.416	...	1.616	14.27	12.4	3.375
090401A	0.45 ± 0.08	0.14 ± 0.05	117.36 ± 5.68	12.96 ± 0.276	0.310	0.114	0.117	109.6	...
090401B	0.06 ± 0.01	0.03 ± 0.01	227.52 ± 17.09	3.12 ± 0.086	0.192	0.105	0.602	156.5	...
090404	1.78 ± 0.30	0.64 ± 0.11	85.84 ± 4.14	20.72 ± 0.644	0.274	0.155	0.715	61.7	...
090407	...	9.63 ± 6.69	147.52 ± 1.02	6.4 ± 0.666	...	0.514	25.54	13.5	1.4485
090410	...	0.64 ± 0.11	167.00 ± 1.43	26.25 ± 0.605	...	0.197	13.446	67.4	...
090418	...	0.64 ± 0.11	57.97 ± 0.85	17.05 ± 0.409	...	0.261	7.604	52.4	1.608
090419	...	0.90 ± 0.15	433.32 ± 5.21	80.04 ± 3.842	...	1.346	207.759	14.3	...
090422	1.26 ± 0.21	0.23 ± 0.14	55.82 ± 9.32	1.16 ± 0.144	0.881	0.405	2.266	16.1	...
090423	1.78 ± 0.30	0.79 ± 0.26	12.36 ± 0.59	3.84 ± 0.147	0.495	0.308	1.211	31.3	8.1
090424	0.12 ± 0.02	0.04 ± 0.03	50.28 ± 0.53	1.98 ± 0.03	0.202	0.095	0.767	131.7	0.544
090429B	...	0.79 ± 0.26	5.80 ± 0.29	1.45 ± 0.079	...	0.319	8.201	22.1	9.4
090509	...	5.58 ± 2.64	293.28 ± 2.76	15.6 ± 1.18	...	0.338	5.731	17.1	...
090510	0.23 ± 0.04	0.12 ± 0.02	0.54 ± 0.08	0.12 ± 0.013	0.762	0.616	0.31	14.9	0.903
090515	0.04 ± 0.01	0.02 ± 0.002	0.07 ± 0.02	0.02 ± 0.004	1.105	0.992	1.285	11.1	...
090516	...	4.39 ± 1.45	228.48 ± 9.45	36.96 ± 2.259	...	0.504	8.23	24	4.109
090518	1.78 ± 0.30	0.64 ± 0.11	45.80 ± 6.71	1.72 ± 0.173	0.606	0.378	0.861	24.1	...
090519	39.04 ± 6.63	19.66 ± 3.34	81.77 ± 6.00	13.69 ± 0.855	0.483	0.494	1.263	15.2	3.85
090530	1.26 ± 0.21	0.64 ± 0.11	40.76 ± 1.15	2.56 ± 0.155	0.554	0.349	0.008	23.7	...
090531A	...	1.73 ± 1.20	45.90 ± 4.91	11.7 ± 0.48	...	0.217	3.284	32.8	...
090531B	1.78 ± 0.30	0.79 ± 0.26	55.52 ± 0.37	2.36 ± 0.155	0.756	0.493	0.442	20.1	...
090618	0.45 ± 0.08	0.14 ± 0.05	115.20 ± 0.43	23.04 ± 0.706	0.071	0.032	0.032	719.8	0.54
090621A	1.26 ± 0.21	0.64 ± 0.11	265.37 ± 1.47	11.56 ± 0.52	0.170	0.118	0.783	67.2	...
090621B	0.08 ± 0.01	0.03 ± 0.02	0.20 ± 0.03	0.06 ± 0.006	0.992	0.675	1.333	13.1	...
090628	7.03 ± 1.19	1.73 ± 1.20	27.70 ± 1.61	2.9 ± 0.186	0.849	0.313	0.618	18.2	...
090709A	0.32 ± 0.05	0.14 ± 0.05	344.85 ± 64.00	28.5 ± 0.471	0.118	0.063	0.115	251.6	...
090709B	7.03 ± 1.19	1.73 ± 1.20	31.20 ± 1.81	4.3 ± 0.262	0.933	0.375	0.64	17.7	...
090712	39.04 ± 6.63	19.66 ± 3.34	169.26 ± 10.06	31.62 ± 1.261	0.686	0.369	0.0005	29.9	...
090715B	...	0.64 ± 0.11	267.54 ± 4.54	15.34 ± 0.587	...	0.134	8.104	84.9	3
090726	...	5.58 ± 2.64	51.03 ± 0.97	9.18 ± 0.574	...	0.390	9.288	17.2	2.71
090727	55.00 ± 9.34	24.36 ± 8.04	300.60 ± 3.90	15.84 ± 1.099	0.857	0.604	0.994	12.3	...
090728	...	7.26 ± 4.32	32.76 ± 3.34	7.02 ± 0.503	...	0.469	3.981	15	...
090807	...	7.26 ± 4.32	151.59 ± 3.76	42.38 ± 2.142	...	0.415	6.657	21.3	...
090809	39.04 ± 6.63	19.66 ± 3.34	192.92 ± 5.24	3.43 ± 0.456	0.893	0.939	0.611	11.8	2.737
090812	0.90 ± 0.15	0.31 ± 0.22	99.76 ± 15.30	18.49 ± 0.516	0.290	0.145	1.34	78.5	2.452
090813	0.32 ± 0.05	0.12 ± 0.02	7.92 ± 0.24	0.99 ± 0.064	0.463	0.324	0.293	28	...
090904A	7.03 ± 1.19	3.54 ± 0.60	162.48 ± 5.26	18.24 ± 0.77	0.424	0.176	2.643	50.1	...
090904B	7.03 ± 1.19	3.54 ± 0.60	58.20 ± 2.40	19.8 ± 0.65	0.230	0.195	1.999	42.6	...
090912	27.70 ± 4.70	5.58 ± 2.64	151.13 ± 8.03	32.13 ± 1.502	0.653	0.200	0.815	33.3	...
090916	2.21 ± 0.73	0.79 ± 0.26	53.20 ± 2.08	3.04 ± 0.291	1.212	1.138	2.693	10.1	...
090926B	...	3.54 ± 0.60	126.36 ± 5.21	21.6 ± 0.621	...	0.235	4.024	63.3	1.24
090927	...	0.64 ± 0.11	18.36 ± 1.33	0.84 ± 0.09	...	0.800	5.846	14.3	1.37
090929B	...	0.12 ± 0.02	371.28 ± 2.42	27.69 ± 1.059	...	0.279	2.927	52.1	...
091018	0.45 ± 0.08	0.18 ± 0.09	4.44 ± 0.15	1.24 ± 0.022	0.245	0.095	2.267	83.3	0.971
091020	1.78 ± 0.30	0.64 ± 0.11	39.00 ± 1.07	6 ± 0.166	0.247	0.130	1.488	55.8	1.71
091024	...	3.54 ± 0.60	114.73 ± 4.95	24.64 ± 0.873	...	0.255	8.486	45.2	1.092
091026	7.03 ± 1.19	1.31 ± 0.78	77.42 ± 6.88	7.14 ± 0.428	0.785	0.192	0.399	30	...
091029	2.51 ± 0.43	1.00 ± 0.48	39.96 ± 1.28	11.47 ± 0.234	0.195	0.105	2.099	68.4	2.752
091102	...	0.64 ± 0.11	7.07 ± 0.14	1.89 ± 0.103	...	0.417	3.454	23.3	...
091112	9.90 ± 1.68	3.54 ± 0.60	27.44 ± 2.09	6.44 ± 0.312	0.581	0.249	0.019	24.1	...
091127	0.23 ± 0.04	0.12 ± 0.02	9.57 ± 0.56	1.54 ± 0.063	0.332	0.228	0.756	50.7	0.49
091130	9.90 ± 1.68	3.54 ± 0.60	388.96 ± 7.62	28.16 ± 1.818	0.747	0.277	0.21	27.5	...

Continued on Next Page...

TABLE 1 – Continued

GRB	Δt_{\min}	Δt_{snr}	T_{90}	T_{R45}	$\sigma_{X,t_{\min}}$	$\sigma_{X,t_{\text{snr}}}$	χ^2/ν	S/N	z
091208A	...	1.31 ± 0.78	80.80 ± 4.87	6.4 ± 0.344	...	0.210	3.732	32.8	...
091208B	0.90 ± 0.15	0.23 ± 0.14	15.21 ± 1.31	1.82 ± 0.121	0.766	0.247	0.291	29.5	1.063
091221	...	0.64 ± 0.11	68.97 ± 2.02	13.2 ± 0.242	...	0.134	5.837	85.1	...
100111A	2.51 ± 0.43	0.79 ± 0.26	15.12 ± 0.96	2.87 ± 0.146	0.766	0.295	0.003	22.9	...
100117A	...	0.64 ± 0.11	638.58 ± 11.62	14.5 ± 1.693	...	1.525	17.319	11.1	...
100212A	0.64 ± 0.11	0.23 ± 0.14	168.70 ± 3.60	5.2 ± 0.261	0.693	0.338	1.574	16.3	...
100213A	0.45 ± 0.08	0.18 ± 0.09	2.37 ± 0.11	0.42 ± 0.028	0.508	0.366	1.972	19.4	...
100305A	...	7.26 ± 4.32	169.99 ± 13.62	28.65 ± 2.318	...	0.669	23.24	13.9	...
100413A	...	3.54 ± 0.60	197.40 ± 2.34	55.46 ± 1.244	...	0.184	4.429	47.7	...
100423A	...	0.06 ± 0.04	115.32 ± 9.82	20.46 ± 0.571	...	0.192	8.861	83	...
100424A	55.00 ± 9.34	19.66 ± 3.34	110.25 ± 5.30	33.6 ± 1.496	0.514	0.283	0.02	24.3	2.465
100425A	...	4.39 ± 1.45	43.56 ± 1.03	2.82 ± 0.251	...	0.680	19.417	14.8	1.755
100504A	4.99 ± 0.85	1.73 ± 1.20	98.07 ± 2.27	10.92 ± 0.403	0.195	0.130	0.176	45.6	...
100513A	39.04 ± 6.63	19.66 ± 3.34	65.10 ± 4.39	18.6 ± 1.022	0.286	0.265	0.085	23.3	4.772
100522A	...	0.12 ± 0.02	35.22 ± 0.32	2.07 ± 0.08	...	0.214	12.353	60.8	...
100606A	...	1.00 ± 0.48	191.73 ± 32.09	16.6 ± 0.891	...	0.276	4.892	41.9	...
100614A	...	40.33 ± 24.01	179.52 ± 12.80	45.76 ± 2.566	...	0.305	6.963	21	...
100615A	...	0.23 ± 0.14	43.46 ± 1.30	9.43 ± 0.222	...	0.084	4.412	107.3	1.398
100619A	0.90 ± 0.15	0.31 ± 0.22	97.90 ± 0.33	8.36 ± 0.203	0.202	0.077	0.19	82.7	...
100621A	1.26 ± 0.21	0.31 ± 0.22	66.33 ± 1.27	19.43 ± 0.327	0.164	0.032	1.806	295.2	0.542
100625A	...	0.03 ± 0.02	0.40 ± 0.06	0.14 ± 0.007	...	0.265	6.59	28.3	...
100702A	0.16 ± 0.03	0.06 ± 0.04	0.52 ± 0.03	0.1 ± 0.01	0.796	0.374	0.891	19	...
100704A	...	0.64 ± 0.11	194.56 ± 4.13	17.44 ± 0.653	...	0.158	4.05	78.1	...
100725A	...	7.26 ± 4.32	151.89 ± 8.15	22.41 ± 1.173	...	0.187	5.831	30.1	...
100725B	...	0.64 ± 0.11	209.92 ± 7.42	26.65 ± 0.538	...	0.179	21.013	94.3	...
100727A	4.99 ± 0.85	1.73 ± 1.20	92.75 ± 4.21	11.25 ± 0.675	0.545	0.192	1.518	31.8	...
100728A	0.23 ± 0.04	0.12 ± 0.02	222.00 ± 6.89	57.35 ± 0.185	0.118	0.089	2.153	296.9	1.567
100728B	4.99 ± 0.85	1.73 ± 1.20	11.52 ± 0.78	2.56 ± 0.142	0.617	0.268	0.213	20.6	2.106
100802A	9.90 ± 1.68	3.54 ± 0.60	564.20 ± 14.25	65.8 ± 2.448	0.709	0.270	0.204	30.6	...
100807A	...	1.00 ± 0.48	8.30 ± 0.45	0.92 ± 0.056	...	0.533	3.168	14.3	...
100814A	...	0.79 ± 0.26	176.96 ± 3.61	31.6 ± 0.749	...	0.089	3.591	98	1.44
100816A	0.23 ± 0.04	0.12 ± 0.02	2.50 ± 0.22	0.84 ± 0.016	0.179	0.148	1.399	58	0.8049
100823A	7.03 ± 1.19	3.54 ± 0.60	18.64 ± 0.93	3.44 ± 0.199	0.752	0.581	2.434	18.4	...
100901A	39.04 ± 6.63	19.66 ± 3.34	459.19 ± 10.66	31.96 ± 2.15	0.722	0.548	0.404	17.8	1.408
100902A	13.95 ± 2.37	4.39 ± 1.45	442.68 ± 4.49	41.85 ± 2.19	0.414	0.192	0.494	33.6	...
100904A	7.03 ± 1.19	3.54 ± 0.60	27.60 ± 2.14	5.98 ± 0.358	0.512	0.473	1.126	19.6	...
100906A	0.64 ± 0.11	0.23 ± 0.14	116.85 ± 0.69	11.07 ± 0.123	0.148	0.071	0.699	135.6	1.727
100924A	...	0.64 ± 0.11	75.84 ± 2.06	13.12 ± 0.323	...	0.245	8.779	67	...
101008A	...	0.79 ± 0.26	9.50 ± 0.18	2.2 ± 0.15	...	0.422	3.079	20	...
101011A	...	1.00 ± 0.48	38.22 ± 1.88	8.58 ± 0.475	...	0.293	3.636	24.7	...
101017A	...	0.06 ± 0.04	78.44 ± 1.85	14.8 ± 0.286	...	0.141	7.878	160.8	...
101023A	0.32 ± 0.05	0.12 ± 0.02	81.64 ± 0.65	10.66 ± 0.153	0.110	0.045	0.009	277	...
101024A	0.23 ± 0.04	0.12 ± 0.02	19.11 ± 0.17	2.31 ± 0.111	0.310	0.200	1.507	44.9	...
101030A	9.90 ± 1.68	3.54 ± 0.60	108.64 ± 3.39	24.64 ± 0.812	0.438	0.164	1.175	43.3	...
101117B	0.32 ± 0.05	0.14 ± 0.05	5.44 ± 0.53	1.2 ± 0.048	0.423	0.259	1.231	37	...
101213A	...	4.39 ± 1.45	175.68 ± 15.30	20.16 ± 0.695	...	0.214	7.832	40.8	0.414
101219A	...	0.12 ± 0.02	0.86 ± 0.06	0.24 ± 0.011	...	0.395	7.509	33.7	0.718
110102A	0.45 ± 0.08	0.18 ± 0.09	271.18 ± 2.13	23.84 ± 0.563	0.138	0.077	2.427	144	...
110106B	...	1.31 ± 0.78	26.68 ± 1.04	8.12 ± 0.306	...	0.308	10.004	29.7	...
110119A	0.90 ± 0.15	0.31 ± 0.22	209.07 ± 1.38	33.81 ± 0.809	0.310	0.152	0.686	84	...
110201A	7.03 ± 1.19	3.54 ± 0.60	13.60 ± 0.66	3.3 ± 0.141	0.491	0.383	0.886	27.8	...
110205A	0.64 ± 0.11	0.23 ± 0.14	277.02 ± 4.67	74.52 ± 0.913	0.219	0.118	1.547	150.4	2.22
110207A	...	0.23 ± 0.14	94.80 ± 4.75	9.6 ± 0.661	...	0.344	3.023	27	...
110212A	...	1.00 ± 0.48	4.65 ± 0.35	1.02 ± 0.058	...	0.313	2.931	18.2	...
110213A	1.78 ± 0.30	0.79 ± 0.26	43.12 ± 3.47	6.44 ± 0.319	0.502	0.276	0.771	31	1.46
110223A	...	19.66 ± 3.34	85.20 ± 4.86	3.04 ± 0.452	...	1.633	6.669	8.5	...
110223B	...	4.39 ± 1.45	64.17 ± 2.55	11.04 ± 1.019	...	0.866	7.41	13.7	...
110315A	...	1.00 ± 0.48	95.13 ± 2.24	23.31 ± 0.762	...	0.239	5.195	42.4	...
110318A	...	0.23 ± 0.14	16.80 ± 0.65	4.2 ± 0.105	...	0.138	25.792	63.2	...

Continued on Next Page...

TABLE 1 – Continued

GRB	Δt_{\min}	Δt_{snr}	T_{90}	T_{R45}	$\sigma_{X,t_{\min}}$	$\sigma_{X,t_{\text{snr}}}$	χ^2/ν	S/N	z
110319A	2.51 ± 0.43	0.79 ± 0.26	20.90 ± 0.71	6.65 ± 0.123	0.366	0.134	0.07	65.6	...
110402A	...	0.18 ± 0.09	108.42 ± 9.73	13.65 ± 0.933	...	0.829	2.735	17.4	...
110407A	39.04 ± 6.63	19.66 ± 3.34	156.04 ± 4.84	44.82 ± 2.244	0.603	0.452	2.396	22.7	...
110411A	9.90 ± 1.68	3.54 ± 0.60	82.77 ± 1.06	24.92 ± 0.704	0.321	0.130	0.062	52.6	...
110412A	9.90 ± 1.68	4.39 ± 1.45	24.45 ± 1.07	5.7 ± 0.245	0.567	0.310	0.471	20	...
110414A	...	5.58 ± 2.64	159.87 ± 4.14	25.55 ± 1.302	...	0.277	2.79	21.9	...
110420A	1.78 ± 0.30	0.64 ± 0.11	15.30 ± 0.95	4.2 ± 0.117	0.391	0.141	0.191	65	...
110422A	0.23 ± 0.04	0.12 ± 0.02	26.73 ± 0.29	9.24 ± 0.09	0.118	0.077	0.626	210.1	1.77
110503A	0.64 ± 0.11	0.18 ± 0.09	9.31 ± 0.64	2.1 ± 0.056	0.341	0.130	1.417	62.7	1.613
110519A	4.99 ± 0.85	1.00 ± 0.48	27.74 ± 0.99	7.22 ± 0.139	0.445	0.071	0.424	73.2	...
110520A	9.90 ± 1.68	3.54 ± 0.60	20.06 ± 0.89	6.12 ± 0.28	0.462	0.253	0.051	25.9	...
110530A	...	9.63 ± 6.69	46.42 ± 2.26	7.04 ± 0.562	...	0.533	3.249	12.7	...
110610A	0.90 ± 0.15	0.31 ± 0.22	54.06 ± 2.17	11.73 ± 0.331	0.265	0.114	0.423	74.8	...
110625A	0.90 ± 0.15	0.18 ± 0.09	64.50 ± 4.25	6 ± 0.15	0.506	0.126	0.241	82	...
110709A	0.23 ± 0.04	0.12 ± 0.02	47.04 ± 1.10	12.48 ± 0.241	0.164	0.110	0.562	149.2	...
110709B	...	0.64 ± 0.11	57.64 ± 1.08	18.48 ± 0.274	...	0.164	8.727	108.1	...
110709B	0.64 ± 0.11	0.23 ± 0.14	267.12 ± 2.24	47.88 ± 0.911	0.212	0.110	0.639	118	...
110715A	0.16 ± 0.03	0.04 ± 0.03	13.15 ± 1.40	1.45 ± 0.025	0.145	0.045	0.107	202.3	0.82
110731A	...	0.12 ± 0.02	46.56 ± 7.14	3.36 ± 0.071	...	0.155	4.02	130.3	2.83
110801A	...	1.73 ± 1.20	400.40 ± 1.99	54.56 ± 1.731	...	0.261	7.97	35.6	1.858
110818A	...	4.39 ± 1.45	77.28 ± 5.61	20.16 ± 0.829	...	0.295	8.552	30	3.36
110820A	...	4.39 ± 1.45	267.92 ± 2.79	9.28 ± 0.649	...	0.648	10.202	16.3	...
110915A	...	0.18 ± 0.09	80.86 ± 0.72	16.12 ± 0.376	...	0.145	7.191	63.3	...
110921A	9.90 ± 1.68	4.39 ± 1.45	33.25 ± 2.00	8.4 ± 0.472	0.674	0.454	1.653	16.5	...
111008A	...	1.00 ± 0.48	75.66 ± 2.25	10.92 ± 0.543	...	0.217	5.976	39.2	4.9898
111016A	19.66 ± 3.34	5.58 ± 2.64	554.58 ± 5.16	74.26 ± 3.229	0.454	0.187	0.705	35.7	...
111022A	...	1.73 ± 1.20	25.60 ± 0.89	6.88 ± 0.219	...	0.122	4.448	40.4	...
111029A	...	1.31 ± 0.78	8.28 ± 0.25	2.79 ± 0.123	...	0.245	28.086	25	...
111103A	1.26 ± 0.21	0.64 ± 0.11	11.83 ± 0.13	2.47 ± 0.108	0.369	0.307	0.714	28.6	...
111103B	...	0.14 ± 0.05	155.74 ± 6.88	9.49 ± 0.226	...	0.100	3.237	119.6	...
111107A	...	1.73 ± 1.20	31.59 ± 2.44	5.46 ± 0.285	...	0.290	5.256	23.1	2.893
111121A	0.08 ± 0.01	0.03 ± 0.02	113.16 ± 6.18	4.16 ± 0.212	0.385	0.224	0.555	37.9	...
111123A	...	3.54 ± 0.60	235.20 ± 6.58	63 ± 1.513	...	0.152	10.182	67	3.1516
111225A	13.95 ± 2.37	5.58 ± 2.64	75.60 ± 2.41	16.65 ± 0.793	0.511	0.277	0.113	21.7	...
111228A	0.32 ± 0.05	0.12 ± 0.02	101.40 ± 1.31	9 ± 0.307	0.305	0.114	0.346	94.9	0.714
120102A	0.32 ± 0.05	0.14 ± 0.05	41.52 ± 18.21	4.08 ± 0.153	0.219	0.110	0.295	97	...
120106A	...	0.79 ± 0.26	66.12 ± 1.26	5.04 ± 0.349	...	0.330	3.676	25.5	...
120116A	1.26 ± 0.21	0.64 ± 0.11	36.08 ± 1.12	8.8 ± 0.159	0.190	0.114	0.103	82.1	...
120118B	...	1.31 ± 0.78	30.78 ± 2.85	8.91 ± 0.336	...	0.235	5.851	30.7	2.943
120119A	0.32 ± 0.05	0.14 ± 0.05	70.40 ± 4.32	13.6 ± 0.198	0.114	0.063	0.366	221.5	1.728
120213A	2.51 ± 0.43	1.00 ± 0.48	38.88 ± 1.53	10.56 ± 0.26	0.179	0.110	2.292	62.4	...
120218A	...	1.31 ± 0.78	33.60 ± 1.03	6.65 ± 0.482	...	0.609	3.189	16.4	...
120305A	...	0.006 ± 0.003	0.76 ± 0.26	0.04 ± 0.002	...	0.290	5.753	31.9	...
120308A	...	19.66 ± 3.34	56.71 ± 3.94	17.49 ± 0.741	...	0.390	13.445	25.1	...
120311A	0.90 ± 0.15	0.23 ± 0.14	3.68 ± 0.28	0.6 ± 0.032	0.825	0.261	1.043	25.9	...
120311B	...	1.73 ± 1.20	32.40 ± 1.76	7 ± 0.354	...	0.322	2.803	24.3	...
120324A	0.32 ± 0.05	0.14 ± 0.05	198.72 ± 22.97	18.86 ± 0.409	0.272	0.138	0.28	124.4	...
120326A	...	0.64 ± 0.11	72.72 ± 3.08	4.68 ± 0.114	...	0.126	3.532	87.2	1.798
120327A	1.26 ± 0.21	0.64 ± 0.11	71.20 ± 2.33	10.2 ± 0.329	0.327	0.182	0.159	63.2	2.813
120328A	...	1.73 ± 1.20	30.24 ± 2.75	6.72 ± 0.421	...	0.490	20.18	17	...
120404A	19.66 ± 3.34	7.26 ± 4.32	40.50 ± 1.49	12.15 ± 0.461	0.556	0.279	0.125	23.2	2.876
120514A	...	1.00 ± 0.48	167.05 ± 1.21	14.82 ± 0.643	...	0.228	5.409	28.8	...
120521B	...	19.66 ± 3.34	78.88 ± 6.86	12.24 ± 0.821	...	0.482	3.636	17.3	...
120521C	3.54 ± 0.60	1.31 ± 0.78	33.18 ± 2.38	5.32 ± 0.236	0.485	0.182	0.66	31.2	...
120612A	55.00 ± 9.34	24.36 ± 8.04	129.80 ± 13.33	27.5 ± 1.447	0.609	0.437	0.627	16.1	...
120624B	0.32 ± 0.05	0.14 ± 0.05	174.72 ± 0.28	38.22 ± 0.302	0.164	0.105	2.071	212.6	...
120703A	0.45 ± 0.08	0.14 ± 0.05	52.83 ± 4.07	3.15 ± 0.151	0.341	0.114	0.032	67.4	...
120712A	...	0.64 ± 0.11	18.46 ± 1.07	4.68 ± 0.146	...	0.316	20.141	40.7	4.1745
120714A	...	4.39 ± 1.45	20.40 ± 1.33	3.8 ± 0.208	...	0.427	2.862	18.1	...

Continued on Next Page...

TABLE 1 – Continued

GRB	Δt_{\min}	Δt_{snr}	T_{90}	T_{R45}	$\sigma_{X,t_{\min}}$	$\sigma_{X,t_{\text{snr}}}$	χ^2/ν	S/N	z
120729A	1.26 ± 0.21	0.64 ± 0.11	78.65 ± 6.50	7.7 ± 0.289	0.207	0.138	0.302	54	0.8
120802A	1.78 ± 0.30	0.64 ± 0.11	50.16 ± 1.52	5.4 ± 0.221	0.458	0.210	0.39	46	3.796
120803B	...	3.54 ± 0.60	46.20 ± 3.07	7.92 ± 0.311	...	0.253	3.317	36.9	...
120804A	0.16 ± 0.03	0.06 ± 0.04	1.78 ± 0.32	0.32 ± 0.015	0.423	0.228	0.894	35.1	...
120811C	1.78 ± 0.30	0.64 ± 0.11	25.20 ± 1.26	6.15 ± 0.129	0.245	0.100	0.056	83	2.671
120815A	...	1.00 ± 0.48	9.68 ± 1.21	1.76 ± 0.145	...	0.479	3.449	14.3	2.358
120907A	2.51 ± 0.43	1.00 ± 0.48	6.27 ± 0.28	1.11 ± 0.065	0.720	0.455	0.872	15.6	0.97
120909A	...	1.31 ± 0.78	617.70 ± 30.95	44.95 ± 2.362	...	0.217	8.982	49.9	3.93
120911A	...	1.00 ± 0.48	22.14 ± 1.44	2.82 ± 0.168	...	0.249	4.206	23.4	...
120913A	2.51 ± 0.43	0.79 ± 0.26	32.20 ± 1.68	3.71 ± 0.185	0.628	0.245	0.851	28	...
120913B	1.78 ± 0.30	0.79 ± 0.26	129.95 ± 1.85	37.95 ± 0.701	0.210	0.114	0.882	96.3	...
120922A	...	0.79 ± 0.26	179.54 ± 6.27	43.93 ± 1.448	...	0.173	5.161	43.2	3.1
120927A	...	3.54 ± 0.60	44.10 ± 3.52	12 ± 0.394	...	0.190	5.714	42.8	...
121001A	77.50 ± 13.16	30.99 ± 14.67	148.75 ± 5.79	34 ± 1.775	0.257	0.263	2.197	20.3	...
121011A	19.66 ± 3.34	7.26 ± 4.32	130.98 ± 14.87	15.34 ± 1.295	0.783	0.335	0.0005	18.6	...
121014A	1.78 ± 0.30	0.79 ± 0.26	58.56 ± 0.43	4.8 ± 0.289	0.632	0.385	0.078	22.3	...
121024A	7.03 ± 1.19	3.54 ± 0.60	12.46 ± 0.39	2.94 ± 0.188	0.356	0.349	1.49	19.5	2.298
121027A	9.90 ± 1.68	3.54 ± 0.60	69.30 ± 1.90	15 ± 0.567	0.604	0.232	0.077	38	1.77
121031A	1.26 ± 0.21	0.64 ± 0.11	118.82 ± 3.72	14.82 ± 0.483	0.187	0.158	2.041	64.1	...
121102A	1.78 ± 0.30	0.79 ± 0.26	33.60 ± 2.67	7.04 ± 0.202	0.230	0.152	1.93	56.1	...
121108A	...	1.00 ± 0.48	46.17 ± 23.31	6.75 ± 0.566	...	0.300	11.583	23.8	...
121117A	9.90 ± 1.68	3.54 ± 0.60	32.62 ± 2.47	6.72 ± 0.304	0.640	0.283	1.611	30.3	...
121123A	3.54 ± 0.60	1.00 ± 0.48	330.88 ± 4.12	48.4 ± 0.759	0.190	0.071	0.021	130.8	...
121125A	...	0.64 ± 0.11	59.16 ± 4.60	15.3 ± 0.465	...	0.288	21.644	69.4	...
121128A	...	0.12 ± 0.02	25.65 ± 5.47	4.75 ± 0.198	...	0.155	2.83	122.3	2.2
121201A	...	1.31 ± 0.78	39.04 ± 2.93	8.96 ± 0.534	...	0.484	17.138	19.7	3.385
121209A	...	0.23 ± 0.14	43.70 ± 0.46	6.9 ± 0.345	...	0.239	3.628	39.7	...
121211A	3.54 ± 0.60	1.31 ± 0.78	184.14 ± 2.31	15.18 ± 1.507	0.537	0.327	0.322	22.3	1.023
121217A	1.78 ± 0.30	0.79 ± 0.26	847.50 ± 12.05	64.75 ± 1.996	0.221	0.148	2.344	47.8	...
130131A	...	4.39 ± 1.45	51.90 ± 0.40	2.6 ± 0.252	...	0.818	8.121	13.7	...
130206A	...	5.58 ± 2.64	115.60 ± 17.20	19.04 ± 1.255	...	0.338	3.412	21.4	...
130215A	...	19.66 ± 3.34	89.05 ± 8.39	19.5 ± 1.148	...	0.561	4.956	19.4	0.597
130216A	...	0.12 ± 0.02	7.12 ± 0.29	2.56 ± 0.059	...	0.232	19.947	77.1	...
130306A	3.54 ± 0.60	1.00 ± 0.48	356.15 ± 11.23	45.05 ± 1.105	0.134	0.045	0.26	156.4	...
130315A	19.66 ± 3.34	7.26 ± 4.32	235.77 ± 3.86	62.33 ± 2.084	0.498	0.173	2.249	37.1	...
130420A	3.54 ± 0.60	1.00 ± 0.48	114.84 ± 4.84	21.56 ± 0.455	0.200	0.071	0.255	100.7	1.297
130420B	...	0.79 ± 0.26	10.36 ± 0.70	2.87 ± 0.131	...	0.237	4.679	29.2	...
130427A	0.06 ± 0.01	0.02 ± 0.002	324.70 ± 2.50	7.64 ± 0.382	0.063	0.032	0.187	635.6	0.3399
130427B	4.99 ± 0.85	1.31 ± 0.78	7.04 ± 0.26	2.24 ± 0.103	0.387	0.241	0.862	23.2	2.78
130502A	0.90 ± 0.15	0.31 ± 0.22	3.09 ± 0.14	0.63 ± 0.04	0.748	0.414	0.968	16.2	...
130504A	9.90 ± 1.68	4.39 ± 1.45	140.94 ± 9.45	20.3 ± 1.476	0.730	0.504	2.598	18	...
130505A	4.99 ± 0.85	1.31 ± 0.78	292.81 ± 33.84	6.23 ± 0.623	0.663	0.302	1.397	26	2.27
130511A	...	0.31 ± 0.22	4.95 ± 0.82	0.57 ± 0.065	...	0.657	7.214	11	1.3033
130514A	1.78 ± 0.30	0.79 ± 0.26	220.32 ± 5.60	34.02 ± 0.871	0.197	0.141	1.507	79.1	3.6
130521A	2.51 ± 0.43	1.00 ± 0.48	12.00 ± 0.67	1.68 ± 0.1	0.669	0.302	0.416	20.1	...
130527A	0.64 ± 0.11	0.23 ± 0.14	73.92 ± 6.86	4.8 ± 0.096	0.355	0.202	2.247	48.1	...
130528A	...	0.64 ± 0.11	652.24 ± 16.89	19.22 ± 0.928	...	0.164	14.596	86.7	...
130529A	...	24.36 ± 8.04	98.58 ± 4.02	27.56 ± 1.362	...	0.324	3.621	19.5	...
130603A	39.04 ± 6.63	9.63 ± 6.69	64.90 ± 2.87	22 ± 0.696	0.367	0.161	0.203	31.9	...
130603B	0.01 ± 0.002	0.005 ± 0.001	0.22 ± 0.01	0.04 ± 0.007	0.396	0.195	0.995	46.9	0.3564
130604A	27.70 ± 4.70	9.63 ± 6.69	78.07 ± 9.81	14.06 ± 0.771	0.493	0.224	0.162	26.1	1.06
130605A	7.03 ± 1.19	3.54 ± 0.60	12.32 ± 0.60	3.08 ± 0.193	0.466	0.492	1.008	16	...
130606A	0.90 ± 0.15	0.31 ± 0.22	278.52 ± 3.54	11.77 ± 0.679	0.414	0.219	0.414	41.7	5.913
130609A	4.99 ± 0.85	1.73 ± 1.20	7.20 ± 0.29	2.32 ± 0.089	0.277	0.200	0.523	27.3	...
130609B	0.90 ± 0.15	0.31 ± 0.22	254.80 ± 6.66	16.8 ± 0.308	0.195	0.084	0.534	108.9	...
130610A	7.03 ± 1.19	3.54 ± 0.60	48.45 ± 2.35	9.31 ± 0.298	0.482	0.221	1.129	46.8	2.092
130615A	153.89 ± 26.13	53.49 ± 37.17	343.10 ± 6.64	69.35 ± 3.716	0.601	0.257	0.357	19.2	...
130625A	13.95 ± 2.37	3.54 ± 0.60	40.64 ± 1.98	12.16 ± 0.525	0.536	0.228	1.749	30.4	...
130627B	13.95 ± 2.37	5.58 ± 2.64	30.40 ± 1.90	7.68 ± 0.45	0.673	0.397	0.03	18.2	...

Continued on Next Page...

TABLE 1 – Continued

GRB	Δt_{\min}	Δt_{snr}	T_{90}	T_{R45}	$\sigma_{X,t_{\min}}$	$\sigma_{X,t_{\text{snr}}}$	χ^2/ν	S/N	z
130701A	...	0.14 ± 0.05	4.62 ± 0.09	1.62 ± 0.034	...	0.134	5.736	71.1	1.155
130722A	1.78 ± 0.30	0.64 ± 0.11	89.40 ± 1.26	20.4 ± 0.288	0.241	0.095	0.336	154.3	...
130727A	0.45 ± 0.08	0.18 ± 0.09	13.86 ± 0.32	4.48 ± 0.084	0.292	0.134	0.197	88.2	...
130806A	1.78 ± 0.30	0.79 ± 0.26	6.27 ± 0.18	1.02 ± 0.062	0.616	0.425	1.524	18.9	...
130807A	...	1.00 ± 0.48	302.25 ± 8.64	55.25 ± 3.981	...	0.422	4.636	21.6	...
130812A	1.26 ± 0.21	0.64 ± 0.11	8.28 ± 0.24	2.07 ± 0.078	0.438	0.355	1.282	33.5	...
130831A	0.64 ± 0.11	0.23 ± 0.14	34.65 ± 0.53	4.07 ± 0.094	0.200	0.071	0.777	92.3	...
130907A	0.06 ± 0.01	0.03 ± 0.01	357.23 ± 2.03	40.31 ± 0.139	0.071	0.045	2.184	801.4	...
130919A	...	19.66 ± 3.34	86.52 ± 4.00	23.52 ± 1.263	...	0.469	16.655	19.9	...
131002B	13.95 ± 2.37	5.58 ± 2.64	54.72 ± 4.12	10.26 ± 0.43	0.631	0.261	2.564	24.7	...

NOTE. — Burst durations (T_{90} and T_{R45}), S/N values, and redshifts were taken from the Butler et al. (2007) catalog (see, also Butler et al. 2010; Butler 2013). Bursts where linear phases in $\sigma_{X,\Delta t}$ could not be fitted by a model with confidence level $> 90\%$, are considered to yield upper limits $\Delta t_{\min} \leq \Delta t_{\text{snr}}$.